Coordination Chemistry Reviews, 117 (1992) 1–43
Elsevier Science Publishers B.V., Amsterdam

ODMR spectroscopy of coordination compounds

Alexander L. Kamyshny[a]*, Arthur P. Suisalu[b] and Leonid A. Aslanov[a]
[a] *Department of Chemistry, Moscow State University, Moscow 119899 (Russia)*
[b] *Institute of Physics, Estonian Academy of Sciences, Tartu 202400 (Estonia)*

(Received 24 July 1991)

CONTENTS

A. INTRODUCTION

Nowadays the photophysics and photochemistry of coordination compounds attract much attention, due to their practical value as effective photosensitizers in solar energy conversion systems [1–3], as non-silver information recording materials [4], and because of the prospects for their application in synthetic photochemical reactions [5,6]. Moreover, research into coordination compounds promises novel information about chemical bonding in metallic complexes.

The many possible types of excited state entail a variety of photoprocesses involving coordination compounds [7–13]. Depending on the electronic structure of a central ion and the mutual disposition of the orbitals of a metal and ligands, the excitation can be localized on the metal (e.g. d,d*-type) or on a ligand (e.g. π,π^*-type), the charge transfer can occur between d-orbitals of a metal and π-orbitals of ligands [14]. For complexes containing different metal ions (M_1–L–M_2), the charge is often transferred from metal to metal (the so-called intervalent transfer [15]). In the case of complexes with different ligands (L_1–M–L_2), inter-ligand charge transfer states can be formed. For example, they are observed in tetrahedral complexes of d^{10}-ions with N-heterocycles and aromatic thiols [16,17]. There also exist states with outer sphere charge transfer to solvent molecules or within ion pairs [18]. The

* To whom correspondence should be addressed.

0010-8545/92/$15.00

luminiscence kinetic investigation of series of complex compounds can provide evidence for two centres emitting simultaneously in an excited molecule [19]. The "double" emission originates either with different ligands, e.g. in $[Rh(bpy)_n(phen)_{3-n}]^{3+}$ $(n = 1, 2)$ [19], or from different orbitals — d,π^* and d,d*, as in $[Ir(phen)_2Cl_2]^+$ [20], or d,π^* and n, π^*, as in $XRe(CO_3)L$ (X = Cl, Br, I; L = 3-benzoylpyridine) [21] and mixed Ru complexes with 2,2′-bipyridylamine and 2,2′-bipyridine (or 1,10-phenanthroline) [22].

The photophysics of coordination compounds differs from that of organic molecules mainly due to the heavy metal effect. Processes which are not accompanied by spin multiplicity changes (internal conversion, fluorescence), have comparable rates, whereas the rates of processes proceeding with multiplicity changes differ considerably. Rate constants for intersystem crossing in metal complexes increase by about three orders of magnitude and are often close to those of the internal conversion (about 10^{12} s^{-1}). Even more noticeable are the differences in phosphorescence rate constants. For organic molecules, rates exceeding 100 s^{-1} are rare, whereas for metal complexes their typical values are 10^4–10^6 s^{-1} and higher [8,23]. The difference is mainly caused by strong spin–orbit coupling (SOC) induced by heavy atoms. The SOC enhancement results in mixing the singlet and triplet states and in disturbing the spin forbiddenness for transitions between states of different multiplicity. It is therefore dubious to use the terms triplet, phosphorescence and intersystem crossing in such compounds [8]. On the other hand, for many complexes the triplet character of the lower excited states with different orbitals is certain [14,24–34].

In order to understand the nature of coordination compound photoexcited states and the photoprocess mechanisms, the structural, magnetic and dynamic properties of these compounds must be analyzed. However, the arsenal of methods for research into the excited states is limited. Spectral and kinetic techniques based on absorption and emission [8,35] are usually applied to study the structure-dynamic characteristics. However, highly resolved spectra are unobtainable for complex molecules by these methods. Moreover, for multicomponent reaction systems these spectra can overlap, making these conventional methods even less informative. In the past decade, time-resolved Raman spectroscopy [36,37] and the spectroscopy of coherent anti-Stocks Raman scattering [38] have been widely applied to structural analysis. They allow one to obtain a vibrational "picture" of an excited molecule and evaluate the changes in its geometry, force constants and bond lengths at photoexcitation.

For a long time, ESR successfully served to probe triplet states [39,40]. Zeeman triplets were optically detected for the first time in 1967 [41–43], and transitions between sublevels in zero field (ZF) in 1968 [44]. That paved the way for a new trend in studying optical and magnetic properties of excited molecules and crystals, i.e. optical detection of magnetic resonance (ODMR). ODMR modifications are described in detail in refs. 45–49.

This review deals with the principal characteristics of the triplet state fine structure and ODMR fundamentals, especially phosphorescence-microwave double

resonance (PMDR) in ZF. This method provides unique information about magnetic, radiative, and structural properties of the triplet. The review also presents the current state and prospects for the ODMR application to the analysis of the triplet states of coordination compounds.

B. FINE STRUCTURE OF THE TRIPLET STATE

The lower triplet state of a molecular system can be obtained in several ways: light excitation within absorption bands corresponding to singlet–singlet transitions followed by intersystem crossing; excitation within the band of singlet–triplet transition; triplet–triplet energy transfer from a suitable donor; and sometimes in the course of a chemical reaction. Due to the relatively long lifetime of the triplet state, emission (phosphorescence) is usually observed in solid matrices where bimolecular deactivation is inhibited. In a series of metallic complexes, phosphorescence occurs in solution at room temperature because of the great decrease in its lifetime (e.g. $Ru(bpy)_3^{2+}$ [50]).

The three-fold degeneracy of the triplet state is not preserved even in the absence of the external magnetic field. Zero-field splitting (ZFS) depends on internal magnetic interactions in the molecule and sometimes on the influence of the environment or the crystal field (ZFS, shown on the right in Fig. 1, no scaling by energy).

The spin angular momentum of the orbitally non-degenerate state is quantized in three orthogonal planes. Therefore in the non-spherical symmetry of the spatial wave function, the triplet energies split into ZF levels (ZFL) determined by spin–

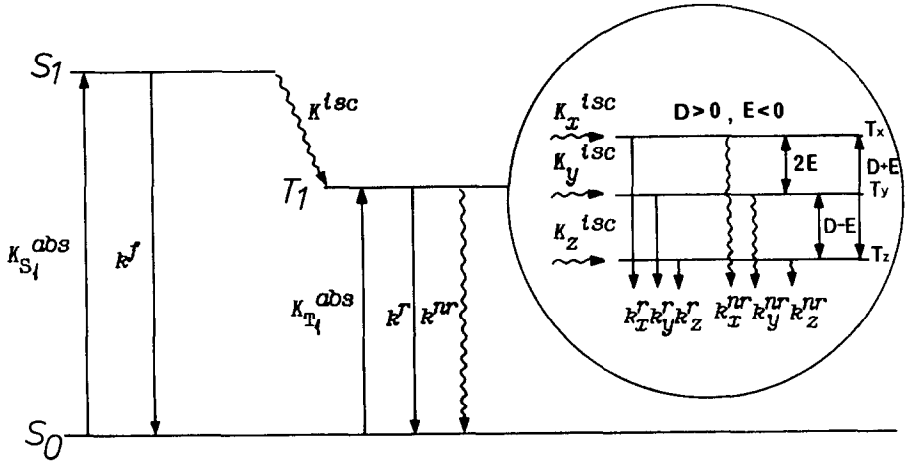

Fig. 1. Five-level scheme of electron states and photophysical processes in molecular systems at photoexcitation (ZFS is shown to the right on a larger scale). Rate constants of photophysical processes are designated as follows: $K_{S_1}^{abs}$ = singlet–singlet absorption; $K_{T_1}^{abs}$ = singlet–triplet absorption; K_i^{isc} = intersystem crossing to the ith ZFL; k^f = fluorescence; k_i^r and k_i^{nr} = radiative and non-radiative decay of ZFL, respectively.

spin dipole interaction (SSI) according to first-order perturbation theory and by second-order SOC [39]. The degeneracy completely vanishes if the molecular symmetry is lower than C_3. Typical SSI-induced ZFS values for aromatic molecules are 0.01 0.3 cm^{-1}, corresponding to microwave radiation energy.

If hyperfine and quadrupolar interactions are neglected, the spin Hamiltonian in ZF can be expressed as [39,40,47]

$$H_0 = \mathbf{S} \cdot \mathbf{T} \cdot \mathbf{S} = -XS_x^2 - YS_y^2 - ZS_z^2 = D(S_z^2 - \tfrac{1}{3}\mathbf{S}^2) + E(S_x^2 - S_y^2) \tag{1}$$

where $\mathbf{S}$, S_x, S_y, S_z are operators of the spin momentum, $\mathbf{T}$ is the second-order tensor whose diagonalization governs the system of principal axes of the triplet fine structure and X, Y, Z are the principal values of the splitting tensor which determine the splitting energy.

The experimental parameters of ZFS (Fig. 1) are equal to

$$D = -\frac{3}{2}Z \tag{2}$$

$$E = -\frac{1}{2}(X - Y) \tag{3}$$

D and E depend on the chosen coordinate system so that, to express the spin Hamiltonian by eqn. (1), they can be positive, negative or have different signs.

It is practically impossible to find out experimentally how much the SSI and the anisotropic portion of the SOC contribute to value of $\mathbf{T}$. The energy of spin sublevels shifts, due to the second-order SOC, by

$$\Delta E_i = \sum_j \frac{\langle \mathrm{T}_i | H_{\mathrm{soc}} | \phi_j \rangle \langle \phi_j | H_{\mathrm{soc}} | \mathrm{T}_i \rangle}{E_{\mathbf{T}_i} - E_{\phi_j}} \tag{4}$$

where T_i are the states corresponding to the ith ZFL of the triplet state, ϕ_j is the perturbing state, H_{soc} is the Hamiltonian of SOC and $E_{\mathbf{T}_i}$ and E_{ϕ_j} are the energies of the corresponding states [39,51]. For multiatomic molecules, H_{soc} is usually approximated by the sum of contributions of certain nuclei [39]

$$H_{\mathrm{soc}} = \sum_{i,k} \xi_k(\mathbf{r}_{ik}) \mathbf{l}_{ik} \mathbf{s}_i \tag{5}$$

where $\mathbf{l}_{ik}$ is the orbital angular momentum operator of electron i about the nucleus k, $\mathbf{s}_i$ is the spin angular momentum of this electron, and the function $\xi_k(\mathbf{r}_{ik})$ determines the SOC value at nucleus k and is related to the mean value of the electric field at a distance $\mathbf{r}_{ik}$ from nucleus k.

Operator H_{soc} has matrix elements of two types: between the electron states of the different and equal multiplicity.

Investigation of carbonyl-containing aromatic compounds shows that the ZFS parameters of the phosphorescent triplet are essentially influenced by SOC between the $^3(\pi,\pi^*)$ and $^{1,3}(n,\pi^*)$ states. It is noteworthy that the selectivity of mixing and

the difference in energies between the interacting states result in a ZFL shift anisotropy and in ZFS enhancement [51–56].

The incorporation of heavy metal atoms in the molecules opens a new route for SOC that involves d-orbitals. In the case of 4d- and 5d-elements in a sum with respect to k of eqn. (5), the contribution of the heavy atom nucleus is predominant, so this equation can be simplified

$$H_{soc} = \sum_i \xi_M(\mathbf{r}_i)\mathbf{l}_{M,i}\mathbf{s}_i \tag{6}$$

where the index M corresponds to a heavy metal atom.

For orbitally degenerate triplet states, the first-order SOC can greatly contribute to ZFS and in non-linear molecules with fairly high symmetry, the triplet fine structure depends on the "competition" between SOC and the nuclear instability of orbitally degenerate states [57].

If no noticeable contribution of SOC to ZFS occurs, the parameters D and E have the obvious physical meaning.

If they are expressed via spatial wave functions [39,40]

$$D = \frac{3}{4}g^2\beta^2\left\langle {}^3\psi\left|\frac{\mathbf{r}^2 - 3z^2}{\mathbf{r}^5}\right|{}^3\psi\right\rangle \tag{7}$$

$$E = \frac{3}{4}g^2\beta^2\left\langle {}^3\psi\left|\frac{y^2 - x^2}{\mathbf{r}^5}\right|{}^3\psi\right\rangle \tag{8}$$

where $\mathbf{r}$ is the vector linking two spins, it can be seen that D depends on the degree of delocalization of the unpaired electrons and decreases with increased delocalization while E is related to the symmetry of the electron distribution function with parallel spins and is equal to zero if the molecular symmetry exceeds C_3. The eigenfunctions of $H_0 - |x\rangle, |y\rangle, |z\rangle$ correspond to states characterized by the processing of the vector of the spin angular momentum in the plane normal to the designated axis, i.e. it is quantized relative to the molecular skeleton, and in ZF a molecule in the triplet state has no magnetic momentum. Here transition $|i\rangle \leftrightarrow |j\rangle$ is polarized along the third axis that can be used in polarization measurements of microwave transitions in oriented molecules [58].

C. SPIN ORIENTATION OF THE TRIPLET STATE

Due to SOC anisotropy, the rates of population and decay of various ZFL depend upon the triplet state pumping both by the scheme $S_0 \rightarrow S_1 \rightsquigarrow T_1$ and the scheme $S_0 \rightarrow T_1$. This leads to the state of so-called spin orientation, non-equilibrium population of sub-levels. The non-equilibrium population can also be achieved by triplet–triplet energy transfer since the pumping rate of the certain ZFL of an

acceptor depends on the populations and projections of the magnetic axes of various ZFL of a donor to the magnetic axes of an acceptor [46].

In any case, the necessary condition for the existence of the non-equilibrium population of ZFL is "freezing" of the spin-lattice relaxation (SLR), when its rate is much lower than that of the triplet state decay. So the spin sublevels can be considered isolated since the triplet lifetime is not long enough for alignment of the populations.

Usually, SLR "freezing" is achieved at a temperature below 4.2 K. Under conventional phosphorescence study conditions (at liquid nitrogen temperature), $kT = 54\ \mathrm{cm}^{-1}$, which exceeds the difference in ZFL energies, and rapid SLR levels their populations. Under these conditions, all spectral-dynamic characteristics of the triplet state are statistically averaged.

If SLR is frozen, the ZFL population at steady-state pumping is expressed by the equation [45,46]

$$n_i^0 = \frac{K_i}{k_i} \tag{9}$$

where K_i is the pumping rate and k_i the total rate of decay of the ith sublevel $(i = x, y, z)$; $k_i = 1/\tau_i$.

The ratio of ZFL populations reflecting the extent of the spin orientation is

$$\frac{n_j^0}{n_i^0} = \frac{K_j k_i}{K_i k_j} \tag{10}$$

K_i can depend on the rate of intersystem crossing $S_1 \rightsquigarrow T_i$ from pumping by the singlet–singlet absorption or on the radiative strength of the process $S_0 \rightarrow T_i$ by direct pumping into the triplet. If pumping is carried out by triplet–triplet energy transfer, K_i depends on the population and the projections of the magnetic axes of the different ZFL of the donor onto those of the acceptor [46].

On switching the excitation off, the population decrease is expressed as

$$n_i(t) = n_i^0 \mathrm{e}^{-k_i t} \tag{11}$$

$$\left(\frac{n_j}{n_i}\right)_t = \frac{K_j k_i}{K_i k_j} \mathrm{e}^{-(k_j - k_i)t} \tag{12}$$

Since each ZFL decays independently, a decrease of the phosphorescence intensity detected at some vibronic band ν after switching the exciting light off is described by a sum of exponents

$$I_\nu(t) = \mathrm{const} + \sum_i A_i \mathrm{e}^{-t/\tau_i} \tag{13}$$

Values A_i depend on the vibronic band type and can be normalized $(\Sigma A_i(\nu) = 1)$.

Thus, under conditions where the rate of SLR is small compared with that of

deactivation of the sublevels, the lifetime of each ZFL contributing to the vibronic band can be evaluated. If more than one component enters eqn. (13), the vibronic band can have mixed polarization (for example, for molecules belonging to C_{2v} and D_{2h} point groups, which are suitable for study by the ODMR method). The direct detection of the phosphorescence characteristics of each ZFL is usually impossible, since the ZFS is less than the non-homogeneous broadening of the spectral bands.

Within the high-temperature region, when SLR is predominant, a Boltzmann distribution of the population between ZFL is set up before phosphorescence appears and is maintained at its decay. In this case, the triplet state behaves as the single level with decay rate [59,60]

$$k = \tfrac{1}{3}(k_x + k_y + k_z) \tag{14}$$

and lifetime

$$\tau = \frac{3}{(1/\tau_x) + (1/\tau_y) + (1/\tau_z)} \tag{15}$$

If $k_x \gg k_y, k_z$

$$k = \frac{k_x}{3}, \quad \tau = 3\tau_x \tag{16}$$

Thus, if only one ZFL contributes to the intensity of the given vibronic band, the lifetime detected at this band at high temperature (usually above 10 K) is three times as high as that at the low temperature. Note that the total population of the triplet state can differ at high and low temperatures [60].

D. FUNDAMENTALS OF THE PMDR METHOD

Perturbation of the triplet state by temperature changes, magnetic field application or microwave radiation can alter the relative population of the ZFL and, consequently, change the relative intensity, polarization and dynamic properties of vibronic bands in the phosphorescence spectra. So, the action of microwaves with frequency corresponding to the energy difference between two ZFLs elicits absorption of microwave energy or its stimulated emission until saturation is achieved, i.e. the alignment of populations of corresponding ZFL. By microwave scanning and detecting the phosphorescence intensity in specific vibronic bands, the PMDR spectrum can be obtained, its resonances being in accord with transitions between ZFL and providing absolute values of the D and E parameters.

As follows from eqns. (2) and (3), $D > 0$, $E < 0$ with the sublevel disposition shown in Fig. 1. However, in general, to find out the signs of D and E and, accordingly, the mutual disposition of T_x, T_y and T_z, independent kinetic and polarization measurements are required.

Analysis of the triplet states by PMDR is possible under the conditions

(1) the triplet state is phosphorescent;

(2) it has spin orientation;

(3) the radiation properties of the ZFL, the populations of which are altered by resonance microwaves, are different; and

(4) the microwave power is large enough to yield noticeable changes in the radiative ZFL population.

Since the extent of spin orientation depends on the excitation mode, the ratio of phosphorescence intensity in the presence and the absence of microwave radiation differs, depending on the excitation mode. El-Sayed has considered the problem in detail [59].

In addition, the intensity ratios also depend on how the microwaves are applied.

Under steady-state optical excitation, according to the scheme $S_0 \rightarrow S_1 \rightsquigarrow T_1$ two methods for ODMR spectra detection are possible, slow or fast passage of microwaves through resonance (action by a saturating microwave pulse is also possible).

In the case of slow (quasi-steady-state) passage, the resonance change of the phosphorescence intensity within the range of transitions $|D|+|E|$, $|D|-|E|$ and $2|E|$ (Fig. 1) is determined by

$$\Delta I = \frac{k_i k_j}{k_i + k_j}(n_i^0 - n_j^0)(\phi_j - \phi_i) \tag{17}$$

where $\phi = k^r/k$ is the phosphorescence yield, and k^r is the probability of emission from the given ZFL.

At the adiabatically fast passage

$$\Delta I = f(n_i^0 - n_j^0)(k_j^r - k_i^r) \tag{18}$$

where f is the inversion factor ($f = 1$ at complete inversion of populations of the sublevels related with resonance frequency, $f = 0.5$ under saturation [61]).

In comparing eqns. (17) and (18), it follows that, in the steady-state regime, the change of signal ΔI is proportional to the difference in emission yields from the pair of levels considered and, in the fast passage regime, to the difference of emission probabilities. In numerous systems, probabilities k^r differ more than yields ϕ, therefore the fast passage method provides a larger useful signal. What is more, this method allows the direct study of kinetics, since after passing through resonance the phosphorescence returns to the non-perturbed intensity in two stages: a rapid decrease of phosphorescence intensity corresponding to devastation of the predominantly emissive state, and slow growth corresponding to population of the state with a long lifetime [62,63].

$$\Delta I(t) = Ae^{-k_i t} - Be^{-k_j t} \tag{19}$$

The meaning of coefficients A and B is clear from Fig. 2, which shows the shape of the transient response curve for decay of the $T_i \leftrightarrow T_j$ microwave resonance.

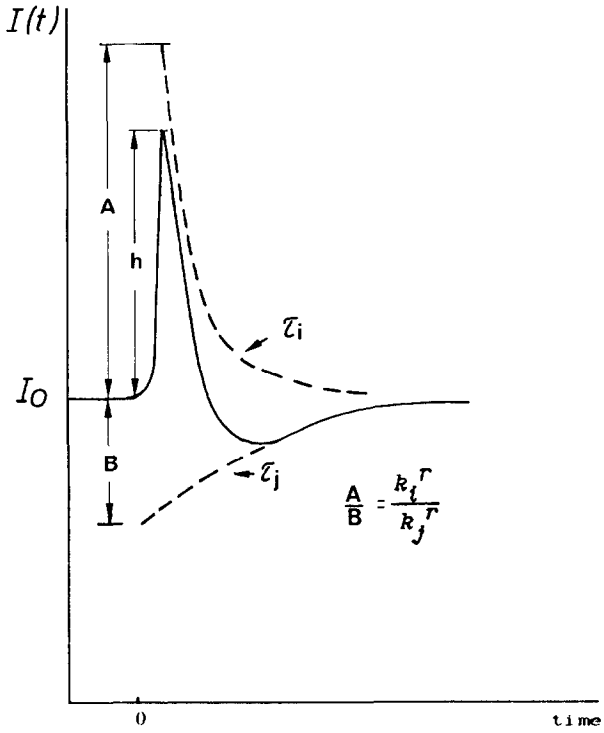

Fig. 2. Transient response curve for transition $T_i \leftrightarrow T_j$ at adiabatically fast passage [62].

Using the adiabatically fast passage method described in detail in ref. 62, one can find total rates of decay of sublevels, their lifetimes and relative rates of radiative deactivation, relative values of steady-state populations, quantum yields, and contributions to emission and populating rates of different ZFL.

Determination of the absolute dynamic characteristics of the ZFL is a rather complicated task. Still, the relative values often adequately interpret ODMR data.

In the above cases, optical excitation is steady-state. However, sometimes this is useless, for instance if steady-state populations are close to one another. In this case, the distinction in ZFL deactivation rates can be utilized, this being the basis of the method of microwave-induced delayed phosphorescence (MIDP). The essence of the method is that, after establishing the steady-state population for each sublevel, the excitation is cut off and each ZFL decays independently. Some time later, the population of the rapidly deactivated sublevel T_i tends to zero (usually at $t \geqslant 5/k_i$) and phosphorescence is defined by the "slower" sublevels T_j and T_k. If a microwave pulse of frequency in resonance with the $T_j \leftrightarrow T_i$ or $T_k \leftrightarrow T_i$ transitions is now applied, the population of the T_i sublevel is enhanced due to the depopulation of one of the two resting sublevels. Since, in general, the "rapid" sublevel has a higher probability of radiation, a growth of phosphorescence intensity is observed, the detected signal

being proportional to the fraction of the population transferred to T_i by the action of the microwave pulse and to the difference in rate constants of radiative decay of resonance-related sublevels.

By varying the delay time after cutting off the optical excitation and applying the microwave field, the complete set of dynamic characteristics of the triplet state is obtained [48,64].

To record weak phosphorescence at strong fluorescence, discontinuous excitation with phosphoroscopic recording should be used.

To take into account the phosphoroscopic method of recording in formulae describing the ODMR effect, the steady-state populations of sublevels n_i^0 must be replaced by effective values $\bar{n}_i$ [63,65]

$$\bar{n}_i = n_i^0 F_i \tag{20}$$

where F_i is the phosphoroscope function

$$F_i = \frac{1}{4} e^{-\delta_i} \frac{\mathrm{sh}(\vartheta_i - \delta_i)}{\vartheta_i \,\mathrm{ch}\, \vartheta_i} \tag{21}$$

and $\delta_i = \Delta/2\tau_i$, $\vartheta_i = T/4\tau_i$, Δ is the recording delay, T is the modulation period.

If the modulation period $T \ll \tau_i$ (and $\Delta \ll \tau_i$), F_i tends to the limit of quasi-steady-state excitation and registration ($F_i \to 1/4$). The multiexponential decay is described by a superposition of separate single-exponential components, their contributions depend on F_i at corresponding τ_i. Following from eqn. (21), the relative contribution of the long components increases and that of the short components decreases. If the decay law depends on wavelength, the circumstances mentioned above must be taken into account upon phosphoroscopic recording of the spectra.

The phosphoroscopic recording method also allows one to record the actual absorption contours of the microwave field at slow scanning. The equation for the quasi-steady-state effect in this case is more sophisticated

$$\Delta I = \frac{k_i k_j}{k_i + k_j} [\phi_i(\bar{n}_j F_{ij} - \bar{n}_i F_i) - \phi_j(\bar{n}_j F_j - \bar{n}_i F_{ji}) + \phi_i \frac{k_i}{k_j} \bar{n}_i (F_{ij} - F_i) - \phi_j \frac{k_j}{k_i} \bar{n}_j (F_j - F_{ij})] \tag{22}$$

where F_{ij} is the phosphoroscope function corresponding to the effective level with average lifetime

$$\tau_{ij} = \frac{2}{k_i + k_j} \tag{23}$$

Comparison of eqn. (22) with eqn. (17) shows that the phosphoroscopic and steady-state optical excitation methods differ due to the discrepancy of τ_i and τ_j of the two spin sublevels related by the resonance frequency of the saturating microwave field. If sufficient time delay, δ_i, is introduced into signal registration, the contribution

of the "fast" component becomes irrelevant (F_i and $F_{ij} \to 0$). In the limiting case, only the component with a long lifetime ($F_j = 0$) is detected and the "purely" steady-state ODMR effect is achieved.

Figure 3 presents the scheme of an experimental installation to record the PMDR spectra. Light from a source (usually Hg or Xe–Hg lamp) falls on a sample passing through focusing optics and a filter. The sample mounted inside a microwave helix is placed in an optical helium cryostat equipped with a pumping system. Microwave radiation transmits from oscillator to the sample through coaxial line. Depending on the helix characteristics, the output power usually varies from several milliwatts to several hundred milliwatts at the conventional steady-state ODMR detection. For the measurement of coherent effects, microwave radiation amplifiers are used.

The emission from a sample according to the 90° scheme is focused on the entrance slit of a monochromator, and a signal from a phototube is directed to the detection system. A double-disc phosphoroscope with constant phase shift is usually employed in our PMDR-spectrometer configuration to avoid interfering fluorescence. A detailed description of the equipment can be found in ref. 48.

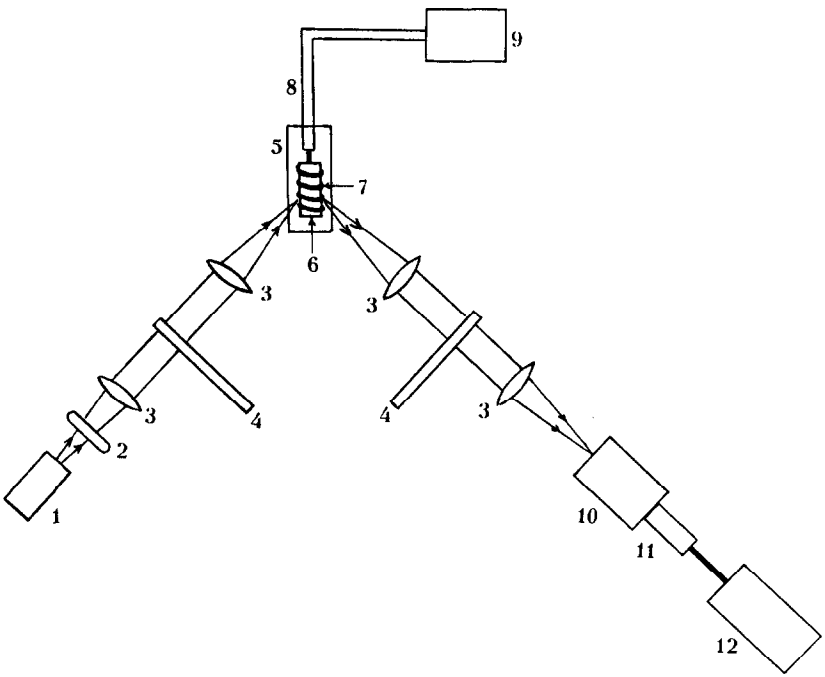

Fig. 3. Scheme of experimental installation for PMDR spectra registration. 1, light source; 2, filter; 3, lens; 4, phosphoroscope discs; 5, cryostat; 6, sample; 7, helix; 8, coaxial line; 9, microwave sweep oscillator; 10, monochromator; 11, phototube; 12, detection electronics.

E. NON-PHOSPHORESCENCE ODMR IN ZERO FIELD

Since steady-state optical pumping leads to different intersystem crossing rates from S_1 to ZFL of the triplet as well as from different ZFL to S_0, one can imagine a situation when T_1 is populated predominantly through one ZFL and is deactivated through another. Upon application of microwave radiation, being in resonance with transitions between these ZFL, the total population of the triplet state falls, whereas the population of S_0, and consequently of S_1, grows. Since all the electronic levels are dynamically related, the change in triplet population under the action of microwave resonance can be detected by any optical transition: singlet–singlet ($S_0 \rightarrow S_1$) or triplet–triplet ($T_1 \rightarrow T_n$) absorption, or fluorescence ($S_1 \rightarrow S_0$) [49,66].

The method of fluorescence-detected magnetic resonance (FDMR) is often employed. It is extremely useful when the molecules do not phosphoresce or their phosphorescence is very weak and occurs in a poorly available IR region.

Phosphorescence detection is more sensitive since the effect is induced by changes in the relative ZFL population, whereas the influence of the microwave field on the intensity of fluorescence or triplet–triplet absorption is determined by changes in the total steady-state population of the triplet state, which is usually low. So, the change of optical signal by fluorescence detection is within 0.1–1% [49,63].

The experimental installation for studying ODMR spectra by non-phosphorescence detection is, in principle, the same as that shown in Fig. 3, but with some variation in the recording system.

F. ADVANTAGES OF ZERO-FIELD ODMR

Let us consider the merits of zero-field ODMR for studying the excited triplet states.

ODMR spectra provide valuable information about magnetic properties and the fine structure of the triplet. ODMR has a number of evident advantages when compared with ESR. First, conventional ESR is inapplicable to the short-lived states (<0.1 s), which makes it virtually useless for the investigation of metallic complexes. Secondly, unlike Zeeman states, one can study zero-field states of the spin Hamiltonian. Here, the triplet spin functions are transformed according to irreducible representations of the molecular point group, which simplifies the analysis. The use of single crystals and the magnetic field is not necessary. Thirdly, ODMR utilizes the more sensitive optical channel for the detection. The increased sensitivity is caused by the fact that the absorption of a microwave quantum under favourable conditions changes the recorded high-energy optical emission by one photon, i.e. enhancement of the energy sensitivity is approximately equal to the ratio of the frequencies of an optical photon and a microwave quantum.

Moreover, detected molecules can be selected optically with high resolution by laser excitation.

PMDR allows identification of the ZFL as the sources of various vibronic bands in the phosphorescence spectra [46]. If, for instance, a single ZFL is the source of the vibronic band, its nature can be determined according to the change in intensity of this band upon saturation of various transitions in ZF. The polarization characteristics of the band remain unchanged. If the vibronic band is emitted from two ZFL, emission from each ZFL has a different polarization characteristic for molecules of suitable symmetry (not too high and not too low). In such a system, the microwave saturation of transitions relating two radiative ZFL slightly influences the phosphorescence intensity of this band but strongly alters the polarization pattern.

The assignment of vibronic bands with different ZFL as well as data extracted from the kinetic investigations on the population rates of ZFL and their radiative and non-radiative deactivation enables interpretation of the spin selectivity mechanism of intersystem crossing, SOC and vibronic SOC, defining the radiative properties of the triplet. Here, ODMR is more promising than time-resolved spectroscopy which provides only absolute rate values.

ODMR methods facilitate the analysis of intermolecular energy transfer pathways. For example, it is feasible to establish whether the transfer occurs by singlet–singlet or triplet–triplet mechanisms since for the former, the intensity of the signals observed should be the same as that at the direct excitation of the acceptor in state S_1. For the triplet–triplet energy transfer, a spatial relation can be established between the spin planes of the donor and the acceptor as well as the spin selectivity of the process [45,46].

The applicability of the ODMR techniques for detecting the geometry of the triplet molecules is based on the possibility of predicting the transition number in ZF as well as the number and symmetry of the ZFL, which phosphoresce on the O,O-band in accordance with molecular symmetry. Comparison of these predictions with experimental data, among them analysis of the vibronic band origin, provides an idea of the triplet geometry. In addition, the parameter E (eqns. (3) and (8)), which is related to the symmetry of the distribution function for electrons with parallel spins, gives information about the triplet geometry. This parameter is very sensitive to alteration of the nature of the low-temperature matrix, which then affords evaluation of the influence of the crystal field on the triplet properties [67]. The other ZFS parameter, namely D (eqns. (2) and (7)), evaluates the degree of delocalization of the unpaired electrons and depends slightly on the crystal field properties.

PMDR can also be useful to identify the triplet states formed by different molecules in a relatively complicated system by the position of microwave resonances. In this case, PMDR works as a qualitative analysis technique. In detecting metallic complex formation, ZFS parameters can be even more sensitive characteristics than the phosphorescence spectra [26].

The spin orientation of the triplet state is manifest in low-temperature photochemical reactions. The spin selectivity has been revealed in reactions of pyrimidine

photodecomposition in benzene at 1.6 K, where microwave radiation with frequency $2|E|$ noticeably decreases the rate of the process [68]. This is caused by the difference in the rate constants of the chemical conversion for different ZFL [69]. Sometimes, the spin orientation explains how the external magnetic field affects photochemical reactions. The influence of this field on relaxation between ZFL is experimentally detected for photochemical reactions in liquids at room temperature [70]. Moreover, triplet-excited molecules in a state of spin orientation can be the products of photochemical reactions [47,71]. This effect is called the chemically induced polarization of electrons. If the above effects are available, ODMR is a fine indicator of photochemical transformations; it identifies their products and provides information on the mechanisms of the reactions of excited molecules [72].

G. ZFS PARAMETERS FOR DIFFERENT TYPES OF COORDINATION COMPOUNDS

Initially ODMR studies with coordination compounds were performed with porphyrin complexes by MIDP [73,74] and by quasi-steady-state ODMR [75].

Porphyrin electronic states and excited state properties are qualitatively interpreted by means of the four-orbital Gouterman model [76]. For metallic complexes with unsubstituted porphyrins of symmetry D_{4h} the orbital nature of the lower excited $^3(\pi,\pi^*)$ state is either $^3(a_{1u} \rightarrow e_g)$ or $^3(a_{2u} \rightarrow e_g)$. These states are degenerate (^3E_u) and compose a set of six ZFL. Under the influence of the crystal field, the degeneracy is eliminated and splitting to two ZFL sets occurs: $|X, T_i\rangle$ (lower state) and $|Y, T_i\rangle$ (upper state) with a distance between their "centres of gravity" 10–100 cm^{-1} [77–79]. Naturally, at low temperatures ESR and ODMR data are related to the lower state.

Within the single set, SSI removes the spin degeneracy and introduces ZFL splitting. SSI between two states can be neglected. Since the lower excited state E_u can have considerable orbital angular momentum relative to axis C_4 (axis z), eqn. (6) can be represented as

$$H_{soc}^{(z)} = \sum_i \xi_M(\mathbf{r}_i) \mathbf{l}_{M,i}^{(z)} \mathbf{s}_i^{(z)} \tag{24}$$

In planar π-systems built of $2p_z$ atomic orbitals, SOC is extremely small [80]. At the same time, with the introduction of metal ions into the centre of the porphyrin ring, a new SOC pathway is open [81,82]; it is caused by the interaction of the d_π-orbitals of the metal with π^*-orbitals of the porphyrin ring where the electron is transferred upon excitation. Non-vanishing matrix elements of H_{soc} in eqn. (24) in basis $|U, T_v\rangle$ (where $U = X, Y$, $v = x, y, z$) can be written in the orbital approximation as [77]

$$\langle X, T_y | H_{soc}^{(z)} | Y, T_x \rangle = \langle Y, T_x | H_{soc}^{(z)} | X, T_y \rangle = \tfrac{1}{2}\mathbf{Z} \tag{25}$$

$$\langle X, T_x | H_{soc}^{(z)} | Y, T_y \rangle = \langle Y, T_y | H_{soc}^{(z)} | X, T_x \rangle = \tfrac{1}{2}\mathbf{Z} \tag{26}$$

$$\langle X, T_z | H_{soc}^{(z)} | Y, T_z \rangle = \langle Y, T_z | H_{soc}^{(z)} | X, T_z \rangle = 0 \tag{27}$$

where **Z** is a constant typical of the central ion.

In fact, matrix elements of eqns. (25) and (26) contain the vibrational wavefunctions of coupled states and when the vibronic coupling is significant, integration over vibrational coordinates leads to the orbital reduction effect [83]. This may be followed by a large decrease in the effective angular momentum and the associated magnetic interactions, among them SOC. To take this effect into account, all the matrix elements are to be multiplied by the same factor **q** and $\mathbf{Z}' = \mathbf{Zq}$ is to be taken instead of **Z**.

If SOC is essentially weaker than the effect of the crystal field, $|X, T_i\rangle$ and $|Y, T_i\rangle$ are the usual triplet states. As follows from eqns. (25)–(27), $H_{soc}^{(z)}$ effectively mixes $|X, T_y\rangle$ with $|Y, T_x\rangle$ and $|X, T_x\rangle$ with $|Y, T_y\rangle$, thus shifting $|Y, T_x\rangle$ and $|Y, T_y\rangle$ upwards, and $|X, T_x\rangle$ and $|X, T_y\rangle$ downwards relative to the corresponding T_z sublevels (Fig. 4) with increase of parameter D by a value D_{soc}. The latter can be evaluated if $\mathbf{Z}'$ and δ (the value of crystal field splitting) are known

$$D = D_{ssi} + D_{soc} \tag{28}$$

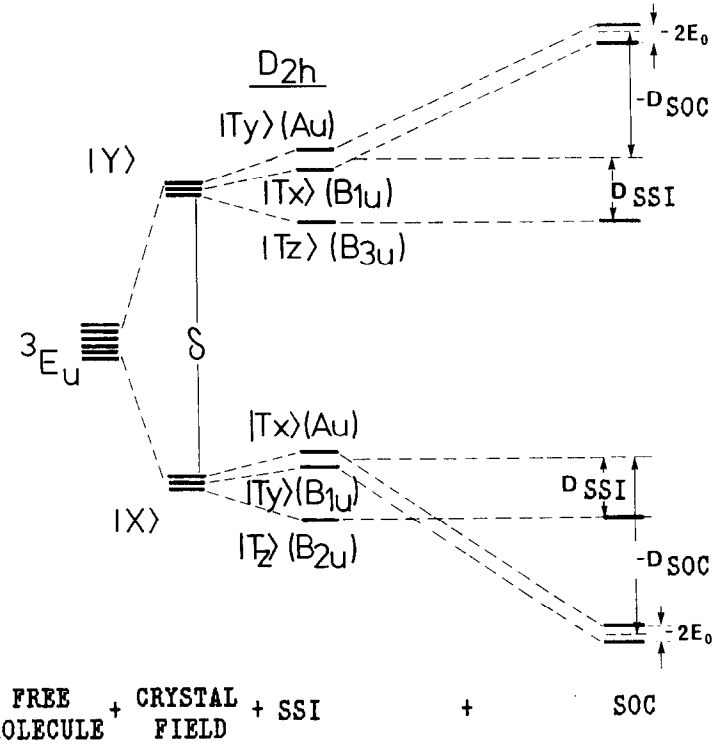

Fig. 4. Energy level diagram of ^3E_u-state of metalloporphyrins when subsequently the crystal field, SSI and SOC are taken into account [84].

$$2D_{soc} = -\frac{\mathbf{Z}'^2}{2\delta} \tag{29}$$

Here, eigenfunctions $|U, T_v\rangle$ contain a slight "admixture" of the functions related with them via SOC.

Metalloporphyrins can be divided into three groups according to the nature of the metal (metals with the filled d-shell, d-elements with an even number of electrons, whose complexes give "pure" triplet states, and metals with unpaired d-electrons).

For the elements with a filled d-shell, such as Zn(II), Cd(II), Sn(IV), Ge(IV), Si(IV), as well as Mg(II) devoid of d-electrons, there is no pronounced contribution of the second-order SOC into ZFS (Table 1); their parameters are close to the corresponding values for free bases: $|D| = 0.0435\ cm^{-1}$, $|E| = 0.0063\ cm^{-1}$ for porphine in *n*-octane [85] and $|D| = 0.0363\ cm^{-1}$, $|E| = 0.0083\ cm^{-1}$ for tetraphenylporphine in the same matrix [86]. This is understandable if one takes into account that effective SOC with (d,π^*)-states is impossible for d^0- and d^{10}-configurations of the central ion.

Interestingly, the lifetime of the triplet state is lower for free porphyrins, compared with their Zn- or Mg-complexes [119], i.e. the SOC effect depending on metal incorporation is weaker in this case than the effect induced by the loss of the N–H bonds whose vibrations are essential for dissipation of the excited state energy. Data on the phosphorescence of octaethylporphyrinate Sn(IV) and Ge(IV) dihalides point out the dominating contribution of halide p-orbitals to SOC [120] and the insignificant role of SOC from the central ion filled d-orbitals. From experimentally detected values δ and calculated values $\mathbf{Z}'$, D_{soc} can be estimated for complexes of Zn(II) with porphine ($\delta = 109\ cm^{-1}$, $\mathbf{Z}' = 0.7\ cm^{-1}$ [75,77]) and Cd(II) with tetrabenzoporphyrin ($\delta = 30\ cm^{-1}$, $\mathbf{Z}' = 1.5\ cm^{-1}$ [90]). These values are $0.0011\ cm^{-1}$ and $0.0188\ cm^{-1}$, respectively, i.e. the contribution of SOC into ZFS for Zn(II) complexes is one order of magnitude less than the SSI contribution and for Cd(II) complexes it is virtually the same.

The deviation of E from zero for all metalloporphyrins shows that the lower triplet state has no C_4 axis, though according to ESR in glasses at 77 K for Zn-porphine $E = 0$, the latter is the consequence of the dynamic averaging of two orbital components ^3E_u [73,78].

ODMR spectroscopy of the various forms of the naturally occurring porphyrin complex Mg(II)-chlorophyll in vitro and in vivo in strains and mutants of photosynthetic bacteria, algae and chloroplasts of higher plants [66] supports the results obtained for the model systems d^{10}-metalloporphyrins: ZFS values are small ($0.01–0.06\ cm^{-1}$) for monomers, dimers and aggregates (Table 1).

ODMR analysis of the structural peculiarities of the primary electron donors in bacterial photosynthesis provides analogous results. In this case, the D and E parameters are also small and fall into a rather narrow interval [79]. Of interest is

TABLE 1

ZFS parameters for coordination compounds[a]

Compound	Matrix	$\|D\|$ (cm^{-1})	$\|E\|$ (cm^{-1})	Method	Ref.
Zn-TPP	*n*-Octane	0.0323	0.0100	PMDR	67
Zn-P	*n*-Octane	0.0360	0.0091	PMDR	73,74
Zn-Etio	*n*-Octane, PMMA	0.0330–0.0354	0.0038–0.0080	PMDR	67,75,87
(Mg-P) · EtOH	*n*-Octane	0.0350	0.0100	FMDR	88
(Mg-P) · Py	Py	0.0321	0.0100	FMDR	89
Mg-TPC	Py	0.0304	0.0075	FMDR	89
Cd-TBP	*n*-Octane	0.0152–0.0330	0.0014–0.0071	PMDR	90
Pd-P	*n*-Octane	0.8130	0.0090	ESR, ODMR	77,84
	n-Octane	0.7672		ESR	91
	n-Decane	1.4010		ESR	91
Si-OEP	*n*-Octane	0.0370	0.0064		78
Ge-OEP	*n*-Octane	0.0400	0.0054		78
Sn-OEP	*n*-Octane	0.0330	0.0040		78
Sc-OEP	*n*-Octane	0.0374	0.0077	PMDR	92
	3-Methylpentane	0.0380	0.0023	PMDR	92
$[Sc\text{-}OEP]_2O$	*n*-Octane	0.0374	0.0037	PMDR	92
	3-Methylpentane	0.0370	0.0070	PMDR	92
Chl *a*	*n*-Heptane	0.0302	0.0044	PMDR	93
Chl *a*	*n*-Octane	0.0280	0.0038	FMDR	94
Chl *a*	PMMA	0.0303	0.0042	ESR	95
Chl *a*	MTHF	0.0288–0.0291	0.0042–0.0054	ESR	95
Chl *b*	*n*-Octane	0.0312	0.0022	FMDR	94
Chl *b*	PMMA	0.00320	0.0032	ESR	95
Chl *b*	MTHF	0.0294–0.0325	0.0029–0.0087	ESR	95
Chl $a \cdot H_2O$	*n*-Octane	0.0309	0.0042	FMDR	96
Chl $a \cdot 2H_2O$	*n*-Octane	0.0291	0.0038	FMDR	96
Chl $a \cdot 2$Py	*n*-Octane + Py	0.0283	0.0040	FMDR	96

TABLE 1 (*continued*)

Compound	Matrix	$\|D\|$ (cm^{-1})	$\|E\|$ (cm^{-1})	Method	Ref.
PChl · H_2O	*n*-Octane	0.0306	0.0071	FMDR	97
Chl *b* · H_2O	*n*-Octane	0.0332	0.0033	FMDR	97
Chl *b* · EtOH	*n*-Octane + EtOH	0.0332	0.0033	FMDR	66
Chl *b* · 2Py	Toluene + Py	0.0293	0.0051	ESR	66
BChl *a* · MTHF	MTHF	0.0226	0.0059	ESR	98
BChl *b*	Py + toluene	0.0212	0.0055	ESR	99
Zn-Chl *a*	*n*-Heptane	0.0304	0.0050	PMDR	93
Zn-Chl *a*	PMMA	0.0296	0.0042	ESR	98
Zn-Chl *a*	*n*-Octane	0.0306	0.0042	ESR, FMDR	100
Zn-Chl *b*	*n*-Octane	0.0328	0.0032	ESR, FMDR	100,101
Cu-Chl *b*	*n*-Octane	0.0396	0.0039	FMDR	101
Cd-Chl *b*	MTHF	0.0326	0.0036	FMDR	101
(Chl *a*)$_2$	Toluene	0.0270	0.0040	ESR	66
(Chl *a* · H_2O)$_2$	*n*-Octane	0.0286	0.0031	FMDR	96
(Chl *a* · H_2O)$_n$	*n*-Octane	0.0275	0.0038	FMDR	96
(Chl *a* · EtOH)$_2$	EtOH	0.0252	0.0039	FMDR	102
(Chl *b*)$_2$	Methylcyclohexane + pentane	0.0281	0.0031	FMDR	103
Zn-Chl *a* · H_2O	Methylcyclohexane + pentane	0.0302	0.0044	FMDR	102
(Zn-Chl *a* · H_2O)$_2$	Methylcyclohexane + pentane	0.0279	0.0038	FMDR	102
$K_2Cr_2O_7$	Single crystals			ESR, PMDR	104–106
	"A-centres"	0.8097	0.0776		
	"B-centres"	0.8940	0.1228		
$KCrO_3Cl$	Crystals	0.9191	0.1636	PMDR	107
$RbCrO_3Cl$	Crystals	0.9398	0.0807	PMDR	107
$CsCrO_3Cl$	Crystals	1.0405	0.1385	PMDR	107
YVO_4	Single crystals	0.0193	0.4576	ESR, PMDR	106,108
$YP_{0.96}V_{0.04}O_4$	Single crystals	0.0374	0.4329	ESR, PMDR	108
$CaMoO_4$	Single crystals	3.1475	1.0907	ESR, PMDR	109

[Zn(2,2′-biquinoline)] · $(ClO_4)_2$	EtOH	0.0863	0.0059	ESR	110
Zn[s-*trans*-6,6′-dimethyl-2,2′-bipyridine] · $(ClO_4)_2$	i-PrOH	0.1012	0.0075	ESR	111
[Zn(bpy)] · $(NO_3)_2$	EtOH	0.1076	0.0056	ESR	26
$[Zn(bpy)_3]$ · $(NO_3)_2$	EtOH	0.1062	0.0058	ESR	26
[Mg(bpy)] · $(NO_3)_2$	EtOH	0.1086	0.0051	ESR	26
[Sr(bpy)] · $(NO_3)_2$	EtOH + H_2O	0.1093	0.0048	ESR	26
[Ca(bpy)] · $(NO_3)_2$	EtOH + H_2O	0.1089	0.0050	ESR	26
$Al(C_{22}H_{22}N_4)$ · Et	MTHF	0.0618	0.0058	ESR	27
$Ge(C_{18}H_{14}N_4)$ · Cl_2	EtOH	0.0827	0.0224	ESR	27
$[Rh(bpy)_3]Cl_3$	EtOH	0.0924	0.0207	PMDR	112–114
$[Rh(bpy)_3]Cl_3$	Single crystals	0.0904	0.0140	PMDR	113,114
$[Rh(bpy)_3]Cl_3$	Crystals	0.0852	0.0175	PMDR	115
$[Rh(bpy)_3]Cl_3$	Crystals	0.0897	0.0175	PMDR	116
$[Rh(bpy)_3]$ · $(ClO_4)_3$	Single crystals	0.0972	0.0197	PMDR	117
$[Rh(bpy)_3]$ · $(BF_4)_3$	Crystals	0.0917	0.0223	PMDR	115
$[Cd(bpy)_3]$ · $(NO_3)_2$	Crystals	0.1144	0.0140	PMDR	115
$[Rh(phen)_3]$ · $(BF_4)_3$	Crystals	0.1321	0.0347	PMDR	115
$[Rh(phen)_3]Cl_3$	Crystals	0.1368	0.0367	PMDR	115
$[Rh(phen)_3]Cl_3$	$[Zn(bpy)_3]$ · $(NO_3)_2$	0.1134	0.0334	PMDR	115
$SnBr_4$(bpy)	CH_3CN	0.1040	0.0038	PMDR	113
$(C_4H_9)SnBr_3$ · (bpy)	CH_3CN	0.1070	0.0078	PMDR	113
$(C_4H_9)_2SnBr_2$ · (bpy)	CH_3CN	0.1060	0.0085	PMDR	113
$(C_2H_5)_2SnCl_2$ · (bpy)	Single crystals	0.1044	0.0068	PMDR	113,118

[a] P = porphine, Etio = etioporphyrin, TPP = tetraphenylporphine, TBP = tetrabenzoporphyrin, OEP = octaethylporphyrin, Chl *a* = chlorophyll *a*, Chl *b* = chlorophyll *b*, TPC = tetraphenylchlorin, PChl = protochlorophyll, BChl *a* = bacteriochlorophyll *a*, BChl *b* = bacteriochlorophyll *b*, bpy = 2,2′-bipyridine, Py = pyridine, MTHF = 2-methyltetrahydrofuran, PMMA = polymethylmethacrylate.

the fact that, for various bacterial photosynthetic systems, the D parameter is on average 20% lower than that for monomeric bacteriochlorophyll in vitro. This can be associated with an increase of the degree of delocalization of the triplet state in the dimer [79].

In the case of porphyrin complexes with metals with partially filled d-shells, the d-levels can be located in the vicinity of singlet and triplet π,π^*-states and thus SOC with involvement of d-orbitals of the central ion becomes possible [77,81,82,84]. Following from eqn. (4), the effect can be rather large due to a small energy gap between the interacting d_π and π^*-orbitals and the high value of H_{soc} (eqn. (24)). So, for the triplet state of Pd(II)-porphine the second-order SOC results in a great enhancement of D [77,84,91]. The evaluation of the SOC contribution to the D value according to eqn. (29) gives D_{soc} equal to 0.9698 cm^{-1} ($\delta = 58\ cm^{-1}$, $\mathbf{Z}' = 15\ cm^{-1}$), i.e. $D_{soc} \gg D_{ssi}$.

If SOC is comparable with or higher than splitting by the crystal field, the orbital angular momentum is only partially quenched and for porphyrin complexes, the formation of three doublets corresponding to different values of the total angular momentum (spin + orbital) is expected; the upper and lower doublets are separated from the mean doublet by $\pm \mathbf{Z}'/2$.

A large energy gap between zero-field states makes it impossible to measure the ZFS parameters by magnetic resonance techniques. According to analysis of the absorption and luminescence spectra of Pt(II)-porphine in hydrocarbon matrices in ZF and in magnetic fields, the $\mathbf{Z}'$ and δ values for this complex are close (76 and 71 cm^{-1}, respectively) and the difference in the energy of doublets is 38 cm^{-1} [121].

For complexes containing metal ions with unpaired electrons, e.g. Cu(II), V(IV)O, Cr(III) with spin $S = m/2$, the singlet states become singmultiplet ($^{m+1}S_1$) and triplet–tripmultiplet (^{m-1}T, ^{m+1}T, ^{m+3}T) as a result of the exchange interaction with the π-system [76,77,82,122]. These states split by exchange d-π integrals, the value of the splitting depending on the porphyrin and metal, varying from dozens to hundreds of cm^{-1} [76]. At low temperature, the ^{m+3}T state usually radiates.

Let us consider the Cu(II)-porphine complex in detail. At temperatures lower than 23 K, its tripquartet state $|^4T_X, m\rangle$ emits (index X indicates that this state is formed from the orbital component $|X\rangle$; $m = \pm 1/2, \pm 3/2$). Since the ground state is a doublet, eight optical transitions are possible for $|^4T_X, m\rangle$; in ZF they are manifest as four pairs of degenerate transitions because of Kramers degeneracies [76,77].

The energy of states $|^4T_X, \pm\frac{1}{2}\rangle$ and $|^4T_X, \pm\frac{3}{2}\rangle$ can be calculated from the equations [77]

$$E_{X,\pm 3/2} = -\frac{\delta}{2} + D_{soc} + D_{ssi} \tag{30}$$

$$E_{X,\pm 1/2} = -\frac{\delta}{2} + \frac{1}{9}D_{soc} - D_{ssi} \tag{31}$$

Since $D_{soc} < 0$, the state $|^4T_X, \pm\frac{3}{2}\rangle$ lies lower than $|^4T_X, \pm\frac{1}{2}\rangle$ by $\frac{8}{9}D_{soc} + 2D_{ssi}$. Direct measurements of the highly resolved luminescence spectra of Cu(II)-porphine in *n*-octane give a value for the ZF splitting in these states equal to about 1.1 cm^{-1} [77]. The radiation ability of states $|^4T_X, \pm\frac{1}{2}\rangle$ and $|^4T_X, \pm\frac{3}{2}\rangle$ is approximately the same and much lower than that of the higher located tripdoublet. Therefore the latter is populated with increasing temperature that is accompanied by an increase in the luminescence intensity and a shift of its maximum to shorter wavelengths with a simultaneous decrease in lifetime of about an order of magnitude.

Van der Waals and co-workers [104–106] investigated the phosphorescent triplet state in single crystals of $K_2Cr_2O_7$ by PMDR (in quasi-steady-state and pulse regimes) and by ESR. This is a charge transfer state from the 2p orbital of oxygen to the d-orbital of the metal. The ZFS parameters exceed those found for organic compounds and porphyrin complexes (Table 1). The definition of the principal axes of the ZFS tensor shows that excitation is localized on one half of the $Cr_2O_7^{2-}$ anion, which is shaped as two tetrahedra with a common vertex, axis z passing through the C_3 axis of the excited fragment with symmetry C_{3v}. At the same time, a deviation of parameter E from zero indicates a decrease in symmetry under the influence of the environment with splitting of the T_x and T_y sublevels which are degenerate at C_{3v} symmetry ($|E| \ll |D|$).

The crystal salts $KCrO_3Cl$, $RbCrO_3Cl$ and $CsCrO_3Cl$ also yield three signals in the ODMR spectra of their charge transfer excited states with D and E parameters exceeding somewhat the corresponding values for $K_2Cr_2O_7$ [107]. The growth of the D parameter with the transition from calcium to the caesium salt can be associated with SOC enhancement.

In the ODMR spectrum of VO_4^{3-}, with a d^0 electron configuration, three signals corresponding to growth of the phosphorescence intensity are observed. The z axis of the ZFS tensor is directed along the V–O bond that testifies to the tendency for anion distortion upon excitation forming a trigonal pyramid, a consequence of the Jahn–Teller static effect [108]. For YVO_4 as well as $YP_{0.96}V_{0.04}O_4$ the T_y sublevels possess the highest energy and sublevels T_x the lowest, which is why $|E|$ considerably exceeds $|D|$.

For another tetraoxo-anion with a $4d^0$-configuration (MoO_4^{2-}) the ODMR and ESR studies are similar in principle, but the ZFL location differs from that for VO_3^{3-}: $T_z > T_y > T_x$. A large increase of $|D|$ upon transition from YVO_4 to $CaMoO_4$ is a result of the SOC enhancement caused by a metal entering the anion composition. A general scheme for splitting the MoO_4^{2-} triplet sublevels is presented in Fig. 5 [109].

Unusually high ZFS values (about 40–50 cm^{-1}) have been obtained from low-temperature spectral and magneto-optical studies of the charge transfer triplet states of a series of Pt(II) complexes, e.g. potassium octaphosphitediplatinate [31,123,124] and *cis*-bis(2-phenylpyridine) platinum [125]. A value of 25 cm^{-1} for the $^3B_{3u}$ state was obtained studying the Zeeman effect for Pt(II) phthalocyanine complexes in Shpolskii matrices [126,127].

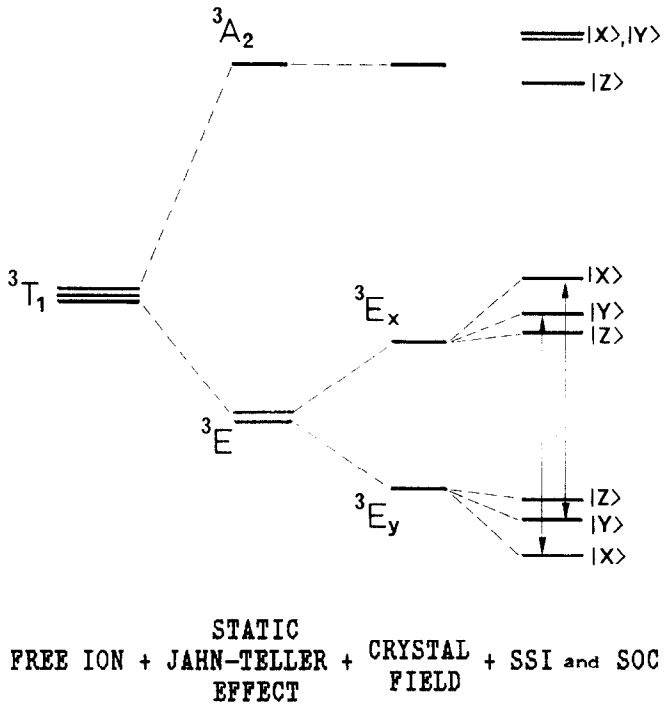

Fig. 5. Energy level diagram of $^3T_1$ state of MoO_4^{2-} when the static Jahn–Teller and crystal field effects, SSI, and SOC are taken into account [109].

Of interest are data obtained by the team of Japanese investigators who analysed the triplet states of 2,2′-biquinoline and 2,2′-bipyridine complexes of Zn(II), Mg(II), Ca(II) and Sr(II) by low-temperature phosphorescence and ESR [26,110]. Phosphorescence lifetimes and the $|D|$ parameters of protonated 2,2′-biquinoline and its Zn(II) complex are close [110], showing virtually no influence of the metal ion on the characteristics of the π,π^*-state of the bound ligand determined by SOC. The situation is the same for complexes with 2,2′-bipyridine [26].

Upon transition from ions with filled shells to ions with a partially filled d-shell, the ZFS increases and tends to grow with increase of the metal atomic number due to enhancement of the SOC contribution. From the widely studied chelate complexes of bidentate nitrogen-containing ligands and a number of other complexes of such metals as Rh(III), Ir(III), Ru(II), the opinion has existed that methods based on magnetic resonance are inapplicable for analysis of the fine structure of their triplet states. The reason is considerable (1–2 orders of magnitude or more) increase in the difference of ZFS energies compared with those of free ligands because of strong SOC [128–130].

The aim of our study is to reveal whether the zero-field ODMR is applicable to investigation of such compounds and to analyze the characteristics of excited

states of complexes with metals of different electronic structures: transition (d-elements), non-transition with closed d-shell and lanthanoids. We have chosen bipyridine complexes of Rh(III), *tris*(2,2′-bipyridine)rhodium(III) chloride, Sn(IV) of general formula $R_nSnX_{4-n}(bpy)$ ($R = C_2H_5$ or C_4H_9, X = Cl, Br, I, $n = 0$–2), and Gd(III), $Gd(acac)_3(bpy)$ and $Gd(NO_3)_3(bpy)_2$.

In low-temperature matrices free 2,2′-bipyridine shows intense phosphorescence from the $^3(\pi,\pi^*)$-state with a lifetime of about 1 s and the O–O band within 23460–23620 cm^{-1} [131–133]. For the Sn(IV) complexes, the presence of the filled d-shell should ensure the localization of the phosphorescent state on a ligand. The same conclusion may be reached for complexes of Gd(III), since the first excited f-shell level ($^6P_{7/2}$) is higher than the ground ($^8S_{7/2}$) by 32200 cm^{-1} [134]; this considerably exceeds the energy of the $^3(\pi,\pi^*)$-state of bound 2,2′-bipyridine. For the complex ion $[Rh(bpy)_3]^{3+}$, localization of the lower excited state on a ligand has been found experimentally [128,135,136].

Figure 6 shows the low-temperature phosphorescence spectra of free 2,2′-bipyridine, $(C_2H_5)_2SnCl_2(bpy)$, $[Rh(bpy)_3]Cl_3$ and $Gd(acac)_3(bpy)$. Analysis of the vibrational structure of the spectra shows, as expected, that the lowest excited state is the $^3(\pi,\pi^*)$-state of the bound ligand (here the O–O band in the phosphorescence spectrum of $[Rh(bpy)_3]Cl_3$ is shifted by 21 nm, Sn(IV) complexes by 12–15 nm, and $Gd(acac)_3(bpy)$ by 6 nm to longer wavelengths). Thus one can study how the nature of the central ion and the composition of the coordination sphere affect the properties of the complex triplet state with the excitation, located on a ligand.

In a single crystal, a molecule of 2,2′-bipyridine has the planar trans-configuration [139] in the ground state. The molecule probably has the same shape in solution and low-temperature matrices [26,140,141] since, according to quantum mechanical calculations, the difference in the energy of trans- and cis-forms is between 2240 cm^{-1} [141,142] and 3390 cm^{-1} [143]. At the same time, there are data concerning the simultaneous existence of two forms of 2,2′-bipyridine in alcohol–water mixtures [141] and in stretched poly(vinyl alcohol) films [26,144].

Here, according to ESR the $|D|$ and $|E|$ parameters are 0.1084–0.1098 cm^{-1} and 0.0045–0.0050 cm^{-1} for the cis-form and 0.1081–0.1104 cm^{-1} and 0.0119–0.0123 cm^{-1} for the trans-form, respectively [26,144,145]. In the PMDR spectra of 2,2′-bipyridine in *n*-heptane, we have observed three doublet resonances: 3.750/3.754, 2.983/2.975 and 0.767/0.779 GHz [112,114] on the O–O band (the latter is shown in Fig. 7).

At high resolution ($\Delta\nu = 3\ cm^{-1}$) the O–O band in the phosphorescence spectrum of 2,2′-bipyridine splits into two lines of about equal intensity with a distance between the maxima of 7 cm^{-1} (Fig. 6). Selective recording of the PMDR spectra on these bands reveals that the doublet resonances belong to optically distinct species in the *n*-heptane matrix. The doublet structure of PMDR as well as the optical O–O transition can be ascribed to different sites or different conformers of guest molecules in this system [133]. The first seems more probable because of the

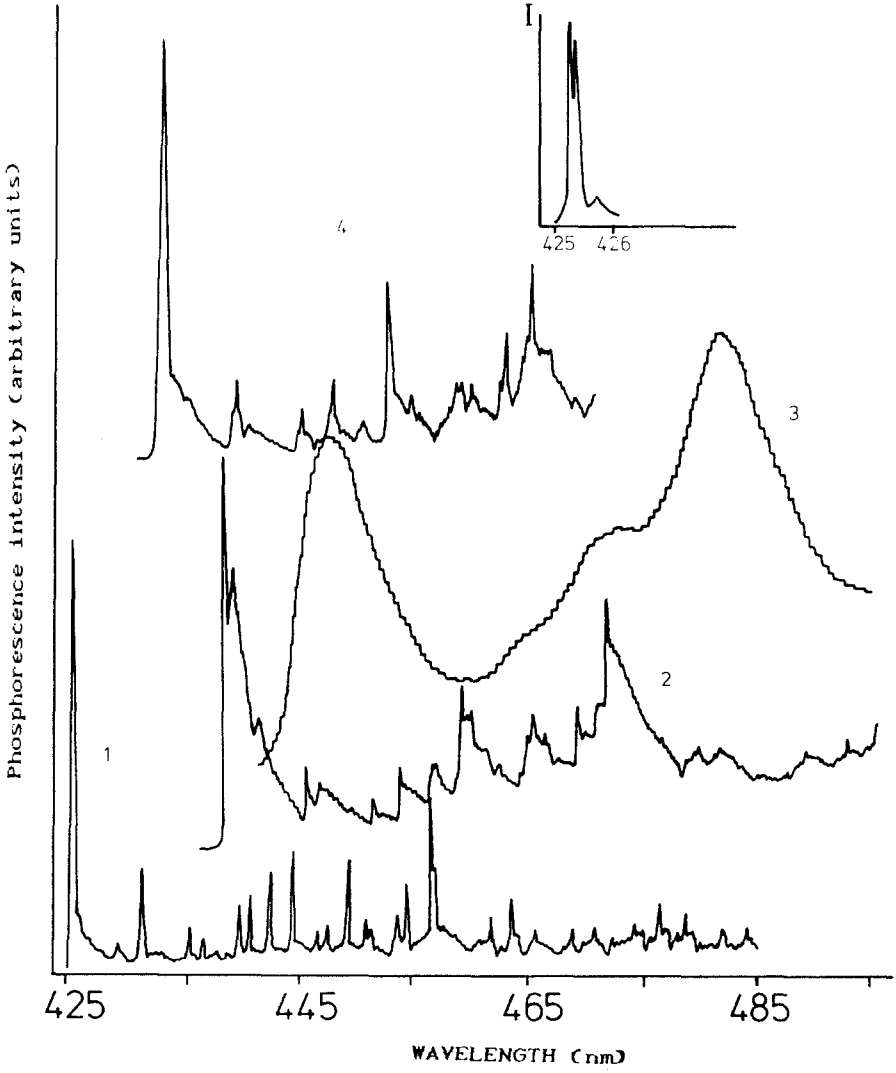

Fig. 6. Phosphorescence spectra of 2,2′-bipyridine in *n*-heptane (1), single crystals of $(C_2H_5)_2SnCl_2(bpy)$ (2), $[Rh(bpy)_3]Cl_3$ in ethanol (3) and $Gd(acac)_3(bpy)$ crystals (4) at 5 K [112,114,137,138]. Top insert shows splitting of the O–O band in phosphorescence spectrum of 2,2′-bipyridine.

higher stability of the trans-form and the similarity of the ground and lower triplet states geometries (the O–O band is the most intense in the phosphorescence spectrum).

In the PMDR O–O band, spectra of the rhodium and Sn(IV) complexes, the resonances are located in the same energy region as for the free ligand (Fig. 7). ZFS

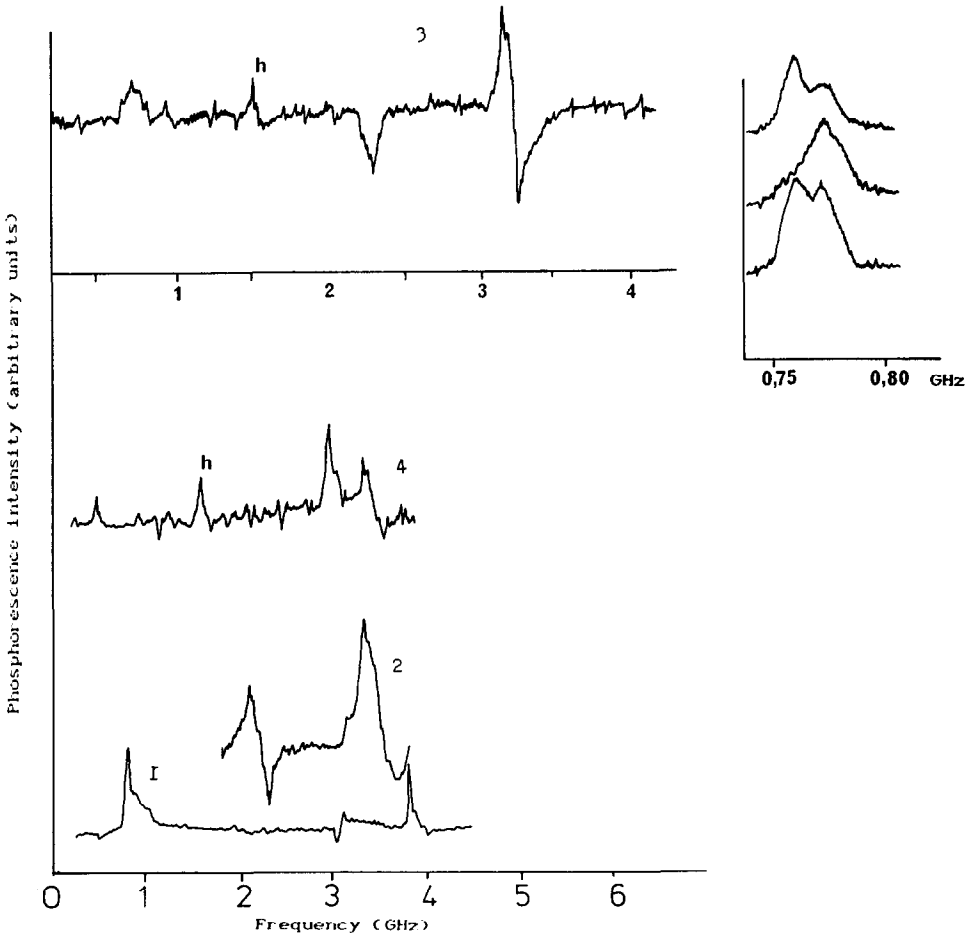

Fig. 7. PMDR signals of 2,2′-bipyridine in *n*-heptane (1), $[Rh(bpy)_3]Cl_3$ in ethanol (2) and in single crystal state (3), and $(C_2H_5)_2SnCl_2(bpy)$ single crystals (4) at 2 K [112–114,118] (the letter **h** designates the second harmonics of $|D|+|E|$ resonance). The spectrum of 2,2′-bipyridine is obtained by the fast-passage method. Top insert shows the doublet resonance for 2,2′-bipyridine and its splitting in steady-state PMDR spectrum.

parameters for the Sn(IV) complexes virtually coincide (Table 1) with the analogous parameters for the cis-form of 2,2′-bipyridine [141,144].

This accords with the conclusion for a very slight contribution of SOC into ZFS for complexes of ions having closed d-shells. Upon transition to $Rh(bpy)_3^{3+}$ with a $4d^6$-configuration, the possibility for an effective $d_\pi-\pi^*$ interaction appears. Such an interaction has been revealed by the X-ray structure analysis of $[Rh(bpy)_3]Cl_3$ single crystals [146] by noticeable shortening of the Rh–N bond (2.025 Å) compared with other Rh(III) complexes with nitrogen-containing ligands, which have no interaction of this kind [81,147,148]. As mentioned above, an anisotropic SOC with the

d,π^* states should greatly increase the ZFS triplet state parameters. Nevertheless our data and those obtained by teams from Japan [115] and The Netherlands [116] show that the SOC is manifest only in a marked (almost 500-fold) decrease of the lifetime of $[Rh(bpy)_3]^{3+}$ triplets.

There is a crude estimation of the SOC contribution to the ZFS parameters of this complex made by Komada et al. [115]. From the expression for the radiative decay rate constant of the triplet

$$k^r_{T_1} = \left[\frac{\nu_{T_1}}{\nu_{S_i}}\right]^3 \left|\frac{\langle T_1 | H_{soc} | S_i \rangle}{E_{S_i} - E_{T_1}}\right|^2 k^r_{S_i} \tag{32}$$

($k^r_{S_i}$ is the radiative decay rate constant of the perturbing singlet state S_i), taking into account that S_i for $[Rh(bpy)_3]^{3+}$, $^1(d,\pi^*)$ is located higher than $^3(\pi,\pi^*)$ by 10 000 cm^{-1}, $k^r_{T_1} = 90\ s^{-1}$ and $k^r_{S_i}$ is equal to that of $[Ru(bpy)_3](BF_4)_2$ ($\cong 10^8\ s^{-1}$), they have obtained $\langle H_{soc} \rangle \cong 16\ cm^{-1}$. The second-order SOC effect on the ZFL energies is given by a modified eqn. (4) [115,149,150]

$$\Delta E_{ij} = |\langle H_{soc} \rangle|^2 \left[\frac{1}{\Delta E_{T_1T_2}} - \frac{1}{\Delta E_{S_iT_1}}\right] \tag{33}$$

where $\Delta E_{T_1T_2}$ denotes the energy difference between the $^3(\pi,\pi^*)$ and $^3(d,\pi^*)$ states ($\cong 8000\ cm^{-1}$). With $\langle H_{soc} \rangle = 16\ cm^{-1}$, eqn. (33) gives $\Delta E_{ij} \cong 6.4 \times 10^{-3}\ cm^{-1}$ ($\cong 0.2$ GHz). This estimation clearly shows that the contribution of second-order SOC to ZFS is negligible.

Analogous estimations for the $[Ru(bpy)_3]^{2+}$ complex ion, the lower excited state of which is characterized by charge transfer from the 4d metal orbital to the ligand π^*-orbital, give the value of the SOC matrix element as $\cong 35\ cm^{-1}$ and the change in the ZF energy of the ith sublevel as $\cong 0.53\ cm^{-1}$ ($\cong 16$ GHz). At the same time, the microwave resonance frequencies in the PMDR spectra of the complexes $[Ru(bpy)_3](BF_4)_2$, $[Ru(phen)_3](BF_4)_2$ and $[IrCl_2(phen)_2]Cl$ fall within the 0.59–4.17 GHz range and no other signals are detected in the region up to 12.4 GHz [150]. These values are very close to the ZFS parameters for the $^3(\pi,\pi^*)$-states with the excitation localized on a bound ligand and contradict the concept of large splitting of triplet sublevels for $^3(d,\pi^*)$ states [128,130].

The low-temperature emission spectra of $[Ru(bpy)_3](PF_6)_2$ and $[Ru(bpy)_3](ClO_4)_2$ crystals reveal the existence of two electronic states resulting from 4d(metal) $\rightarrow \pi^*$(bpy) transitions. These states lie only several wavenumbers apart. When these were investigated by zero-field ODMR on the zero-phonon lines, Yersin et al. [151] also obtained several signals in the range 0.2–6.0 GHz, while their number, location and intensity depend on the choice of the detected zero-phonon line and the nature of a counterion. These results, in the authors' opinion, are consistent with the model of two nearly degenerate doublets (parents of E representa-

tion in D_3 site symmetry) which split by about 0.1 cm^{-1}, the microwave resonances occurring between these doublet sublevels.

Our experiments on the optical detection of magnetic resonances in complexes of the f^7-element gadolinium have yielded rather unexpected results. First, the PMDR spectra resonances are observed at 5 K and practically disappear when the temperature is lowered to 2 K. Secondly, there are seven resonances, not three as in the case of the usual triplet state (Fig. 8). These results can be explained in the following way. Owing to the Coulomb exchange interaction between the Gd^{3+} f-electrons with zero orbital momentum and the ligand π-electrons, the triplet state splits into three tripmultiplet states depending on the total spin, viz. tripoctet ($S = 7/2$) and degenerate tripsextet ($S = 5/2$) and tripdectet ($S = 9/2$) with a splitting of 11 cm^{-1} between them, demonstrated by the quasi-linear phosphorescence spectra of $Gd(acac)_3(bpy)$ (Figs. 6 and 9). This value is considerably smaller than the energy of the Coulomb exchange d–π interaction for copper-containing porphyrin complexes (> 100 cm^{-1} [76]). SSI between f- and π-electrons leads to splitting of the lowest degenerate state to sublevels according to the constant momentum of the f-electrons. Transitions between these sublevels in ZF agree with PMDR spectra resonances (Fig. 9). Since the resonance-related sublevels have similar radiative decay rates, the microwave transitions are detected only with a temperature increase to 5 K, when the tripoctet is sufficiently populated. The latter is in dynamic equilibrium with the lower states and has a high emission quantum yield (lifetimes of the $^{10}T_1$ and $^6T_1$ states exceed 150 ms, lifetime of $^8T_1 \cong 4$ ms). Analogous results were obtained for $Gd(NO_3)_3(bpy)_2$.

All seven PMDR signals for analogous complexes of gadolinium with 1,10-phenanthroline are negative, i.e. the phosphorescence intensity decreases at resonance because of the higher radiative ability of the lower states [152].

H. TRIPLET STATE DYNAMICS OF COORDINATION COMPOUNDS

ZF ODMR experiments alone cannot unequivocally determine the direction of the principal magnetic axes of a molecule and the signs of D and E. Usually, these investigations are performed with strong magnetic fields. However, such data can be provided by combined analysis of the position of the microwave resonances, excitation polarization and phosphorescence, as well as by ZFS dynamic properties. Knowledge of the dynamic characteristics of the triplet state, i.e. rates of population and decay (radiative and non-radiative), enables interpretation of the spin selectivity mechanisms of photophysical processes and gives valuable information on the symmetry of the molecules in the triplet state. It is often sufficient only to know the relative values of the photophysical process rates.

According to ESR, in the strong field, for free porhyrin bases, $D > 0$ and $E < 0$, if the direction of the y magnetic axis is chosen along the N–H bonds and the direction of the z axis, normal to the planar molecule; here, the splitting energy has the following order: $-Z > X > Y$ [78,153].

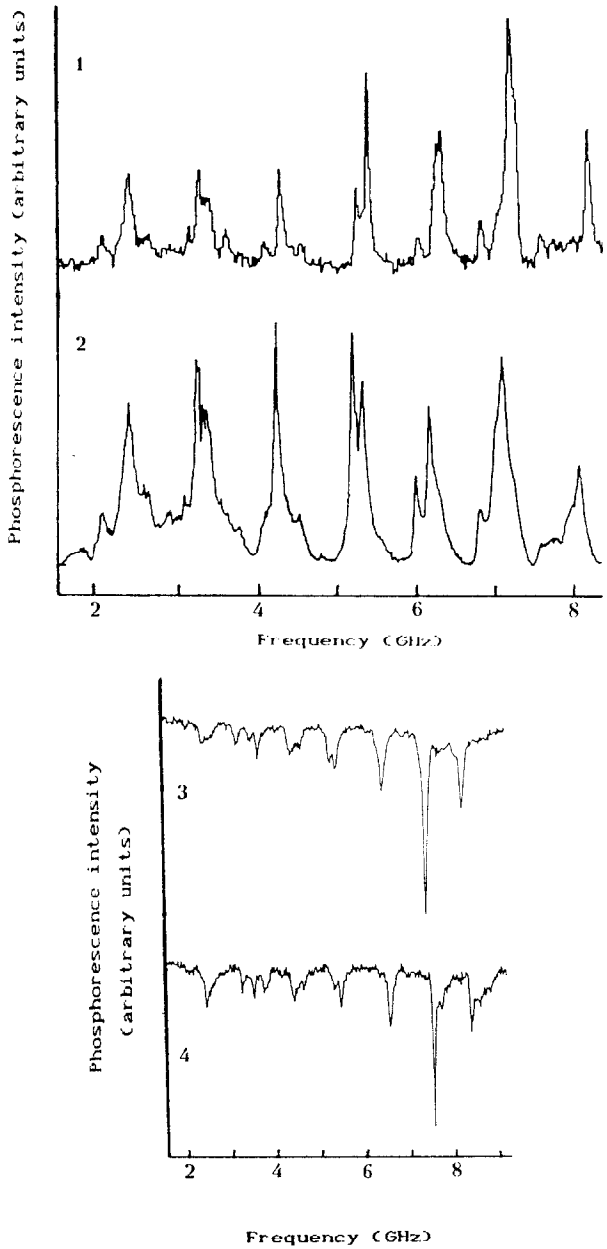

Fig. 8. PMDR signals of $Gd(acac)_3(bpy)$ (1), $Gd(NO_3)_3(bpy)_2$ (2), $Gd(acac)_3(phen)$ (3) and $Gd(NO_3)_3$-$(phen)_2$ (4) in crystal state at 5 K [138,152].

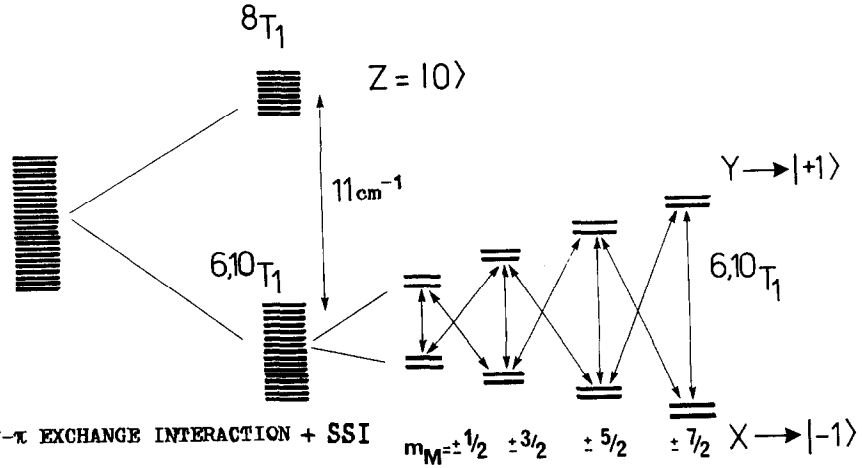

Fig. 9. Energy level diagram of $Gd(acac)_3(bpy)$ triplet state when the f-π exchange interaction and SSI are taken into account. Arrows mark microwave transitions corresponding to the resonances shown in Fig. 8.

The free porphyrin bases and their Mg(II)-complexes show very low phosphorescence (quantum yield $\ll 0.01$) but have high quantum yields for intersystem crossing; the major route for decay of their triplet states is a non-radiative transition [119] and FMDR is the predominant method for studying the fine structure and dynamics [49,66,78]. Table 2 shows that the $^3(\pi,\pi^*)$-states of free porphyrins as well as their Mg(II)-complexes, including the naturally occurring pigments chlorophylls *a* and *b*, behave as typical planar aromatic molecules with heteroatoms: the deactivation rates of the in-plane sublevels greatly exceed the deactivation rate of sublevel T_z. The same situation is observed for the intersystem crossing rates $S_1 \rightsquigarrow T_1$, T_y having the highest activity in all cases. Distinctions in ZFL populations determined by the ratio of the population and decay rate constants are less significant and, according to ref. 97, for chlorophylls *a* and *b* these populations are practically the same. Relatively small differences in the molecular structure of the chlorophyll *a* molecule compared with chlorophyll *b* (substitution of CH_3 by CHO) lead to marked differences in the triplet decay rates [94].

For bacterial photosynthetic systems, the k_x and k_y values greatly exceed k_z, whereas the difference in the population rates for the triplet sublevels is not so pronounced compared with those for plant pigments (mean values of p_x, p_y and p_z for photosynthetic bacteria are 1.0, 0.78 and 0.44, respectively [79]).

Another picture is observed in the case of porphyrin complexes with heavy metal d-shell ions. For Zn-porphine, the phosphorescence yield is about 1% [88], and sublevel T_z is the most active in the radiative and non-radiative decay. The total decay rates of T_x and T_y are close, though T_y does not emit [74,88]. The population rate of T_z is also much higher than that of T_x and T_y leading to the high population of the out-of-plane sublevel. Analogous results have been obtained for Zn-etiopor-

TABLE 2

Dynamic characteristics of the triplet states of coordination compounds[a]

Compound	Matrix	k_x (s^{-1})	k_y (s^{-1})	k_z (s^{-1})	k_x^r	k_y^r	k_z^r	p_x	p_y	p_z	n_x^0	n_y^0	n_z^0	Ref.
H_2P	*n*-Octane	75	230	6.0				0.46	1.0	0.015	1.0	0.71	0.51	154
H_2TPP	*n*-Octane	168	692	50				>0.24	1.0	>0.07				86,155
(Mg-P)·EtOH	*n*-Octane	20	20	2.0				1.0	0.90	0.08				88
Mg-P	Py	32	32	5.0										89
Mg-TPC	Py	139	149	55										89
Chl *a*	*n*-Heptane	400	435	67	0.82	1.0	0.22	0.96	1.0	0.08	1.0	1.0	0.63	93
Chl *a*	*n*-Octane	661	1255	241				0.30	1.0	0.10				94,100
Chl *a*	*n*-Octane	435	500	50							1.0	0.97	0.92	97
Chl *a*	MTHF	400	1250	50							1.0	0.97	0.92	97
Chl *a*	MTHF	400	1250	200				0.47	1.0	0.20				100
Chl *a*	EtOH	710	2710	370				0.38	1.0	0.15				100
Chl *b*	*n*-Octane	268	570	34				0.30	1.0	0.0				94,100
Chl *b*	*n*-Octane	250	330	30							0.98	1.0	0.96	97
Chl *b*	MTHF	270	570	40				0.60	1.0	0.07				100
Chl *b*	EtOH	310	850	65				0.40	1.0	0.10				100
Ca-Chl *b*	*n*-Octane	207	480	32										101
Zn-P	*n*-Octane	4.9	5.9	9.0	0.16	0.0	1.0	0.03	<0.04	1.0	0.06	<0.05	1.0	74
Zn-Etio	*n*-Octane	4.1	3.6	6.1	0.12	0.16	1.0	0.29	0.19	1.0				87
Zn-Chl *a*	*n*-Octane	346	330	660										100,102
Zn-Chl *b*	*n*-Octane	122	250	622				0.3	0.70	1.0				100
Cd-Chl *b*	MTHF	370	462	722										101
(Chl *a*-H_2O)$_2$	Methylcyclohexane + pentane	732	980	180										102
(Zn-Chl *a*·H_2O)$_2$	Methylcyclohexane + pentane	525	585	1220										102
$K_2Cr_2O_7$	Single crystals													106
	"A-centres"	2857	1136	172										
	"B-centres"	909	2272	303										

YVO_4	Single crystals	4000	625	1538										108
$YP_{0.96}V_{0.04}O_4$	Single crystals	2857	303	714										108
$CaMoO_4$	Single crystals	5555	278	33333										108,109
2,2′-Bipyridine	*n*-Heptane	3.2	0.8	0.0	1.0	0.49	0.0				0.73	0.55	1.0	114
2,2-Bipydine	Durene	1.3	2.1	0.25	1.0	0.38	0.073							156
$[Rh(bpy)_3]Cl_3$	EtOH	120	160	1110	0.09	0.15	1.0	0.80	0.63	1.0	1.0	0.61	0.14	114
$[Rh(bpy)_3]Cl_3$	Single crystals	200	270	1110	0.20	0.40	1.0	0.38	0.34	1.0	1.0	0.66	0.47	114
$[Rh(bpy)_3]Cl_3$	Crystals	580	100	170	0.20	0.59	1.0							115
$[Rh(phen)_3]Cl_3$	Crystals	16	60	45	0.09	1.0	0.90							115
$[Rh(phen)_3]Cl_3$	$[Zn(bpy)_3]\cdot(NO_3)_2$	14	30	35	0.23	0.90	1.0							115
$(C_2H_5)_2SnCl_2$ ·(bpy)	Single crystals	1.0	5.0	23	0.0	0.33	1.0	0.05	0.11	1.0	1.0	0.50	1.0	118

[a] k_i = total decay rate constants, k_i^r = relative radiative decay rate constants, p_i = relative population rates, n_i^0 = relative populations.

phyrin [87]. The increased activity of sublevel T_z in the decay process is confirmed by data obtained for chlorophylls *a* and *b* after replacement of Mg by Zn [100,102]. At the same time, sublevels T_x and T_y of the Zn-tetraphenylporphine triplet state are more active in non-radiative decay than T_z [78].

The regularities revealed for porphyrin complexes of Zn(II) are preserved, in general, for related complexes of the heavier metals: Cd(II) and Pd(II) [77,90,91,101].

Data on phosphorescence polarization support the predominant contribution of the T_z sublevel to the radiative decay of heavy metal porphyrin complexes. The polarization value for Zn- and Cu-mesoporphyrins, Zn- and Cu-tetrabenzoporphyrins, and Cu-tetraphenylporphine is positive ($\cong 1/7$) and independent of the excitation wavelength; this provides evidence for the orientation of the oscillator within the molecular plane [157]. Similar data have been obtained for Pd-porphine [91].

Consider the mechanisms which govern the spin selectivity for photophysical processes in porphyrin complexes.

The rate of the non-radiative decay of the *i*th triplet sublevel to the isoenergetic vibrational level of the ground state is described by the Fermi "golden rule"

$$k_i^{nr} = \frac{2\pi}{\hbar} |\langle T_i | H' | S_{0,v} \rangle|^2 \rho(E) \tag{34}$$

where H' is the perturbation Hamiltonian associated with the population transfer from T_i to the ground state (it may be identified with SOC Hamiltonian); $\rho(E)$ is the density of the final states [158,159]. In the spin Born–Oppenheimer approximation, eqn. (34) can be presented as

$$k_i^{nr} = -\frac{2\pi}{\hbar} |C_i^{(0)}|^2 \mathrm{FC} + \frac{2\pi}{\hbar} |C_i^{(1)}|^2 \mathrm{FC} + \frac{2\pi}{\hbar} |C_i^{(2)}|^2 \mathrm{FC} \tag{35}$$

where FC is the Franck–Condon factor and is a function of the energy gap between the lower triplet and the ground state (it is identical for all sublevels); $C_i^{(0)}$ contains the direct SOC matrix elements between T_i and S_0; $C_i^{(1)}$ contains matrix elements of vibronic SOC induced by Herzberg–Teller coupling in one spin manifold; $C_i^{(2)}$ includes the higher order vibronic coupling.

The relative efficiency of the non-radiative decay of the spin sublevels of the lower triplet can be determined by identification of the lowest-order term in eqn. (35), which gives one-centre SOC integrals [159]. Let us turn to free bases and magnesium complexes. According to symmetry considerations, $C_i^{(0)}$ is equal to zero for T_x and T_y; $C_i^{(1)}$ is the lowest-order term giving one-centre SOC integrals for these sublevels. Judging from symmetry considerations, T_z for planar aromatic molecules without a centre of inversion can be related to S_0 via $C_z^{(0)}$ and, in the presence of a centre of inversion, via $C_z^{(1)}$ by means of SOC with $^1(\pi,\pi^*)$, but there are no one-centre terms in both cases, and $C_z^{(2)}$ is the lowest-order expression giving the one-centre integral in the evaluation of k_z, which determines the predominant activity of T_x and T_y in

the triplet state decay [78]. A higher efficiency for T_y in intersystem crossing is also understandable ($k_y > k_x$, $p_y > p_x$).

Of the three states $^1(\sigma,\pi^*)$, $^1(\pi,\sigma^*)$ and $^1(n,\pi^*)$ related via SOC with $^3(\pi,\pi^*)$, the $^1(n,\pi^*)$ state with non-bonding orbitals directed along the x axis possesses the lowest energy in the free base molecules. It is this state which mainly contributes to SOC governing the activity of the T_y sublevel in intersystem crossing. Upon binding of Mg^{2+}, the non-bonding nitrogen atom orbitals involved in the formation of σ-bonds with the metal are stabilized and the energy of the $^1(\sigma,\pi^*)$ states increases. As a result, k_y noticeably decreases (see data for H_2P and Mg–P in Table 2). The value k_x falls to a lesser degree and its decrease can reflect the efficiency of N–H bond vibrations for free base triplet state decay [89].

The prevailing activity of the T_z sublevel in the population and depopulation of the triplet states of heavy metal porphyrin complexes is explained by the fact that their d_{xz} and d_{yz} orbitals have symmetry suitable for mixing with atomic p_z orbitals of the porphyrin system. In this case, $C_z^{(1)}$ is the lowest-order term providing the one-centre SOC integrals with the low-lying state $^1(\pi,\pi^*)$. The decrease in activity of the T_x and T_y sublevels is associated with an increase of the energy of the $^1(\sigma,\pi^*)$-states, which interact with these sublevels by the SOC mechanism. The heavy atom effect is clearly shown on comparing the Zn and Cd complexes where the rate of depopulation of all three triplet sublevels [100,101] increases with atomic number.

The higher deactivation rate of the Mg-porphine triplet state compared with Zn-porphine [74,89] can be explained by the different transition involved. In accordance with the four-orbital Gouterman model [76], the lower triplet state of free porphine and its Mg complex is determined by the transition $a_{2u} \rightarrow e_g$, and for Zn-porphine $a_{1u} \rightarrow e_g$ in symmetry D_{4h} [88,154]. The triplet state corresponding to the transition $a_{2u} \rightarrow e_g$ is deactivated more rapidly due to more effective interaction with C–H bond vibrations of the porphyrin skeleton [88]. The higher rates for the non-radiative deactivation of the T_x and T_y sublevels of the triplet state of Zn-tetraphenylporphine with transition $^3(a_{2u} \rightarrow e_g)$, compared with Zn-etioporphyrin with transition $^3(a_{1u} \rightarrow e_g)$, can be similarly explained [78].

The axial ligands greatly influence the dynamic characteristics and mechanisms of spin selectivity of porphyrin complexes. The presence of two such ligands (e.g. water molecules) in the chlorophyll *a* molecule decreases the mean values of k_x and k_y to a greater extent than k_z and can lead to inversion of the activities of the T_x and T_y sublevels in intersystem crossing [95] with simultaneous change of the relative steady-state populations ($n_z^0 > n_x^0, n_y^0$) [96]. These results are clear from the scheme in Fig. 10. According to the SOC polarization data in pheophytin and metal–pheophytin molecules, the selection rules for the symmetry group C_{2v} are valid [160]. Chlorophyll *a* with one axial ligand has a lower triplet state of $^3B_2$ symmetry (Fig. 10(a)) and none of the sublevels can be directly coupled with the lower singlet $^1B_2$ symmetry. (T_z is populated by means of SOC with S_2 having symmetry $^1A_1$, and T_x and T_y with higher-lying singlet states of orbital nature differing from π,π^*.)

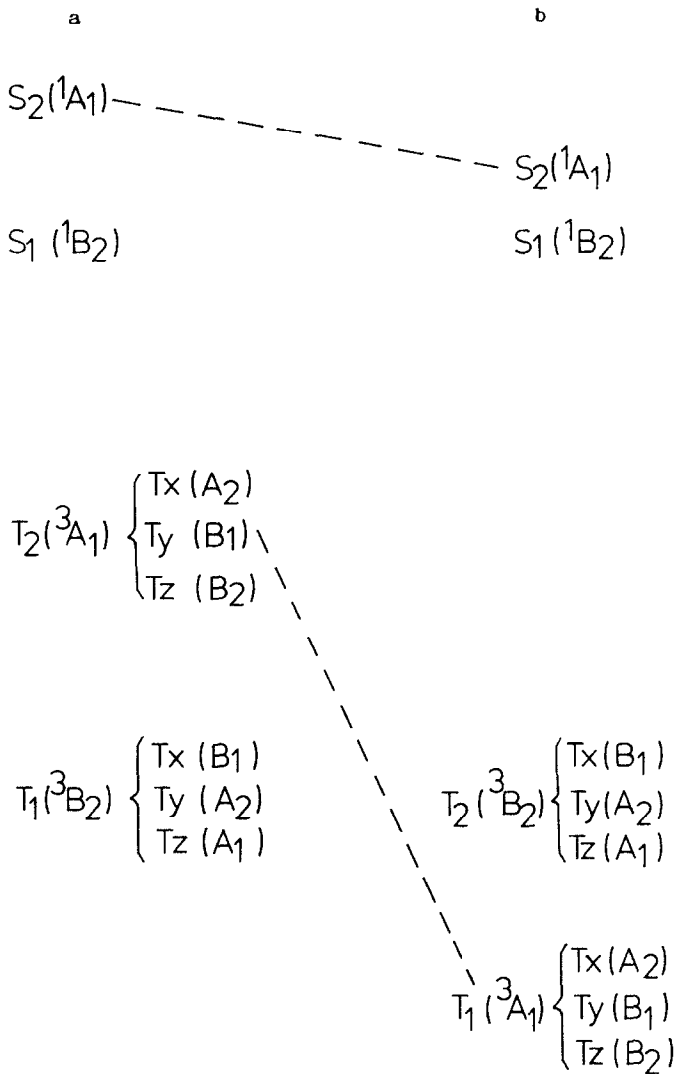

Fig. 10. Energy level diagram of chlorophylls with one (a) and two (b) axial ligands [160,161].

Attachment of the second axial ligand shifts S_2 and T_2 down, with inversion of the order of disposition of the lower triplet states [161]. As a result, the energy gap between S_1 and T_1 increases; this lowers the triplet yield and increases the fluorescence yield. Direct SOC between $S_1(^1B_2)$ and $T_z(B_2)$ is possible and this leads to the experimentally observed relative enhancement of p_z and k_z compared with p_x, p_y and k_x, k_y. In addition, inversion of the symmetry of T_x and T_y of the lower triplet state leads to the alignment or even inversion of the p_x and p_y values for chlorophyll with two axial ligands, versus chlorophyll with one axial ligand [66].

Macrocyclic complexes of Al(III) and Ge(IV) with dibenzotetraaza[14]annulene: $Al(C_{22}H_{22}N_4)Et$ and $Ge(C_{18}H_{14}N_4)Cl_2$ show a clear analogy with the porphyrins both by the structure and by the presence of the coupled π-system with localization of the lower excited $^3(\pi,\pi^*)$-type state on a ligand. Time-resolved ESR revealed that, in this case, the in-plane T_x and T_y sublevels (axis x is directed along the line connecting the centres of benzene nuclei) are populated most effectively.

At the same time, pronounced differences exist between the electronic structures of triplet states of the macrocycle and porphyrins. Quantum mechanical calculations show that about 70% of the unpaired spins in dibenzotetraaza[14]annulene are localized on two trimethine bridges and nitrogen atoms [27], whereas for the porphyrins, delocalization occurs throughout the entire molecule [76].

The $^3(\pi,\pi^*)$ triplet state of the bound ligand is the lowest triplet state in Rh(III) and Sn(IV) complexes.

At 2 K, under conditions of SLR freezing, the phosphorescence decay kinetics of 2,2′-bipyridine in *n*-heptane is described by the sum of two exponents with lifetimes of 0.31 and 1.3 s, which characterize two isolated spin sublevels of the triplet state [114].

Analysis of the microwave resonance decay at the O–O transition by the fast-passage method has shown that, of the three triplet sublevels, only two are radiative; the short-lived sublevel is characterized by an energy of 2247 MHz, and its radiative ability is twice as high as that of the long-lived sublevel with energy 739 MHz (Table 2, Fig. 11).

The most stable form of the lowest triplet state of 2,2′-bipyridine, as well as of the ground state, is the trans-form with the symmetry ^3B_u [140,141], though with a mutually orthogonal disposition of the pyridine rings, the ^3A and ^3B states are almost degenerate [141].

According to the selection rules for the point group C_{2h}, all three sublevels of the triplet, rather than two as observed in our experiments, should radiate in the O–O transition. The emission from all ZFL has been demonstrated [156] by simultaneous application of fast-passage and MIDP methods (the lifetime of the long-lived sublevel is 4 s, $k_{rel}^r = 0.073$). Since the phosphorescence polarization is negative and independent of the wavelength of the exciting light in the region of the singlet $\pi \rightarrow \pi^*$ transitions [162], the in-plane T_x and T_y sublevels are radiative. These sublevels correspond to precession of spins in the yz and xz planes with the direction of the dipole transitions parallel to the z axis. Relative populations of these sublevels are 32 and 24%, respectively. This conclusion accords with data for other planar aromatic molecules with a low-lying $^3(\pi,\pi^*)$-state [46], which facilitates the choice of ZFL location for the free ligand in favour of a scheme with $D < 3|E|$ $(X > -Z > -Y)$ as shown in Fig. 11(a). The disposition of the x axis at an angle to the bond linking the pyridine rings is in line with the known data on the absorption polarization of a trans-form of 2,2′-bipyridine in stretched polyethylene films [163]. The absence of emission from the T_z sublevel (or at least a very small contribution of the sublevel

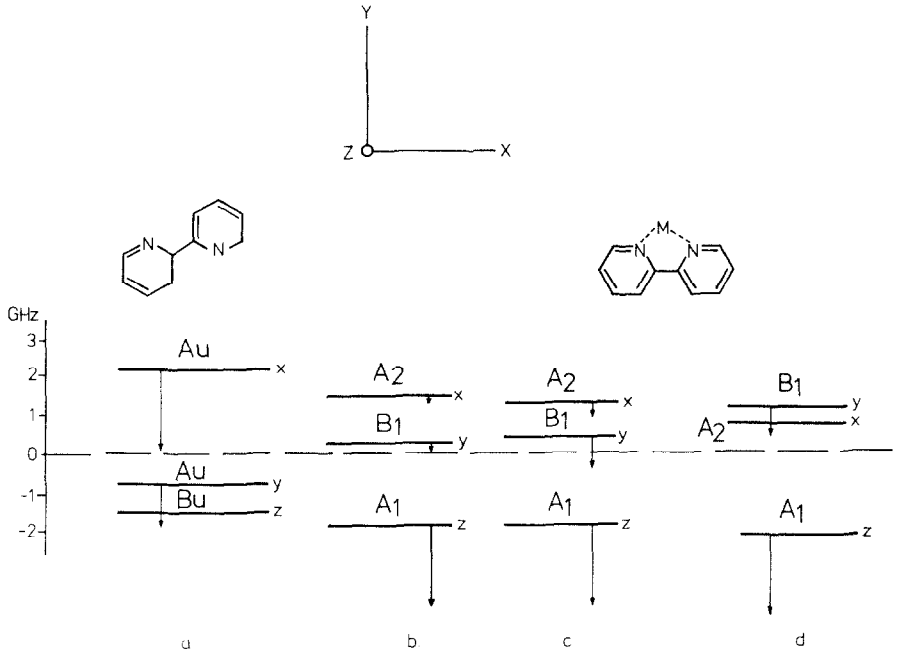

Fig. 11. Diagram of ZFS and dynamic properties of 2,2'-bipyridine in *n*-heptane (a), $[Rh(bpy)_3]Cl_3$ in ethanol (b) and in single crystal state (c), and $(C_2H_5)_2SnCl_2(bpy)$ single crystals (d). The lengths of the arrows correspond to the relative radiative decay rate constants.

to the total intensity) is explained by the fact that the mixing of the $^3(\pi,\pi^*)$- and $^1(n,\pi^*)$-states, which determines the phosphorescence intensity of planar molecules with heteroatoms [164], is effective only for in-plane sublevels with total symmetry A_u and ineffective for the T_z (B_u) sublevel.

For $[Rh(bpy)_3]^{3+}$ in ethanol at 2 K, analysis of the microwave resonance decay kinetics gives three lifetimes for the triplet sublevels: 0.9, 6.2 and 8.1 ms. The ZFS energies of these sublevels are 1845, 305 and 1545 MHz, and their relative radiation probabilities are $k_1^r:k_2^r:k_3^r = 1.0:0.15:0.09$. For the single crystal $[Rh(bpy)_3]Cl_3$, the ZFL lifetimes are 0.91, 3.7 and 5.0 ms, the splitting energies 1807, 484 and 1323 MHz and $k_1^r:k_2^r:k_3^r = 1.0:0.40:0.20$ (Fig. 11, Table 2).

X-ray analysis shows that the structure of this complex ion is characterized by a planar conformation of the ligands with local symmetry C_{2v} for the fragment including one chelate ligand and the metal, and with overall D_3 symmetry [146]. The question of the symmetry of the excited state, namely whether it is located on one ligand or delocalized along the whole coordination sphere, has been argued for a long time [19]. The deviation of the parameter E from zero [114,115], i.e. the absence of degeneracy of the in-plane sublevels, is evidence in favour of the localized excited state (C_{2v}) and the molecule fragment presented in Fig. 11 should be considered for interpretation of the results. In this case, with a cis-configuration of the

ligand molecule, the symmetry of the lowest excited state of $^3(\pi,\pi^*)$-type is $^3B_2(\pi_{a_2}, \pi^*_{b_1})$ [115,165,166]. In accordance with the selection rules, the in-plane $T_x(A_2)$ sublevel should be non-radiative in the O–O transition and phosphorescence should be determined by emission from the $T_y(B_1)$ and $T_z(A_1)$ sublevels with polarization along the z and y axes, respectively; this corresponds to the scheme of sublevels pictured in Fig. 11(b) and (c).

This result is unusual for planar π-systems but can be explained if a d,π^*-state contribution is taken into account. In addition to its dipole-forbidden character, the T_x sublevel has no $^1(d,\pi^*)$-state with analogous symmetry for spin-orbit mixing since the t_{2g} orbitals of the central ion are transformed as a_1, a_2 and b_1 in the C_{2v} point group. Radiation from the T_y and T_z sublevels is determined by SOC with $^1(d,\pi^*)$-states with the symmetry $B_1(d_{a_1}, \pi^*_{b_1})$ and $A_1(d_{b_1}, \pi^*_{b_1})$, respectively, and the difference in their radiative activity on the O–O transition is determined by the difference in the oscillator strengths of the intermediate singlet states. The state with $A_1(d_{b_1}, \pi^*_{b_1})$ symmetry has the higher radiation rate due to larger spatial overlap of the interacting orbitals. In another intersystem crossing process, population of the lower triplet state, the out-of-plane T_z sublevel also has the highest efficiency. Contrary to the results of Komada et al., who discovered that the maximal rate of the total decay is inherent in the T_x sublevel [115], our data [114] show the positive correlation of total and radiative rates. The ratio of decay and population rates is such that the most radiative sublevel has the lowest population and the high population of the weakly radiating T_x and T_y sublevels (57 and 35%, respectively, for $[Rh(bpy)_3]Cl_3$ in ethanol) leads to a large total phosphorescence contribution from these sublevels (55%).

For the $[Rh(phen)_3]^{3+}$ complex ion, $k^r_z(O–O) \cong k^r_y(O–O) > k^r_x(O–O)$. The similar rate constants for emission from the T_y and T_z sublevels can be caused by the superposition of two triplet state configurations, $^3B_2(\pi_{b_1}, \pi^*_{a_2})$ and $^3B_2(\pi_{a_2}, \pi^*_{b_1})$, with the contribution from the first one being predominant; for the SOC matrix elements responsible for emission from T_z, there exist cross terms with a negative contribution to the diagonal terms, and this causes a decrease of k^r_z [115].

The $R_nSnX_{4-n}(bpy)$ complexes show non-exponential phosphorescence decay kinetics at 77 K with a mean rate of 10–1000 s^{-1}. Here, the excited state lifetimes show clear dependence on the nature of the halogen; they decrease with transition from chlorine to iodine. As the temperature falls to 1.8 K, the decay curve shape remains practically unchanged, indicating relatively rapid SLR. Therefore for virtually all complexes of this type, only two microwave resonances can be clearly detected within the range 2.9–3.5 GHz. They correspond to the $|D| + |E|$ and $|D| - |E|$ transitions. Dynamic sublevel characteristics were determined sufficiently accurately only for $(C_2H_5)_2SnCl_2(bpy)$ [118].

Data in Table 2 show that the ZFL parameters for the $^3(\pi,\pi^*)$-type triplet states of Rh(III) and Sn(IV) complexes are rather similar. At the same time, lack of effective spin–orbit coupling with $^1(d,\pi^*)$-states in $4d^{10}$-shell Sn(IV) complexes leads to quali-

tative changes in the disposition of the sublevels and their dynamic characteristics. The mean lifetime of the excited state and the lifetime of the most radiative sublevel in $(C_2H_5)_2SnCl_2(bpy)$ is enhanced by about 50-fold compared with the rhodium complex. Since the highest resonance value (3.33 GHz) corresponds to transition between the most radiative sublevels, and the T_x sublevel in symmetry C_{2v} does not radiate, the triplet fine structure agrees with a disposition of the T_x and T_y sublevels, which is opposite to that for $[Rh(bpy)_3]Cl_3$. The higher radiative ability of the T_z sublevel correlates with the data for Rh(III) complexes.

I. PERSPECTIVES

Thus, research into metal complexes by ZF ODMR reveals not only the applicability but also the high information content of this approach to the analysis of photoexcited states of such compounds. Further investigation will study more triplet state types, including the intraligand, metal-to-ligand and intervalent charge transfer. The method can also be very promising in the study of polynuclear complexes.

The zero-field ODMR experiments are performed almost exclusively at liquid helium temperature. However, it has recently been shown that quite a high degree of triplet state polarization can be reached at liquid nitrogen temperature before relaxation processes equalize the ZFL populations, if short pulse lasers and microwave pulses of sufficient power are used [48,167–169]. The principal condition is that the triplet state should be generated and analyzed within a short period compared with the SLR time. Of special significance are coordination compounds, since the lifetimes of their triplet states are shorter than those of organic triplets. The feasibility of using ODMR spectroscopy at liquid nitrogen temperature and perhaps even at room temperature has great promise in studying the photophysics and photochemistry of solids [48].

REFERENCES

1 K.I. Zamaraev and V.N. Parmon, Usp. Khim., 49 (1980) 1457.
2 Yu.A. Buslaev, A.T. Falkenhoff and V.S. Pervov, Koord. Khim., 8 (1982) 867.
3 A. Harriman, Photochemistry, 16 (1985) 537.
4 H. Hennig and D. Rehorek, Coord. Chem. Rev., 61 (1985) 1.
5 G.G. Wubbels, Acc. Chem. Res., 16 (1983) 285.
6 M.S. Wrighton, J. Photochem., 25 (1984) 63.
7 P.D. Fleischauer, A.W. Adamson and G. Sartori, Prog. Inorg. Chem., 17 (1972) 1.
8 J.N. Demas, J. Chem. Educ., 60 (1983) 803.
9 N. Sutin and C. Creutz, J. Chem. Educ., 60 (1983) 809.
10 F. Scandola and V. Balzani, J. Chem. Educ., 60 (1983) 814.
11 J.F. Endicott, J. Chem. Educ., 60 (1983) 824.
12 A. Cox, Photochemistry, 16 (1985) 165.
13 A. Cox, Photochemistry, 16 (1985) 188.

14 G.A. Crosby, J. Chem. Educ., 60 (1983) 791.
15 C. Creutz, Prog. Inorg. Chem., 30 (1983) 1.
16 K.A. Truesdell and G.A. Crosby, J. Am. Chem. Soc., 107 (1985) 1787.
17 G.A. Crosby, R.G. Highland and K.A. Truesdell, Coord. Chem. Rev., 64 (1985) 41.
18 V. Balzani, N. Sabbatini and F. Scandola, Chem. Rev., 86 (1986) 319.
19 M.K. DeArmond and C.M. Carlin, Coord. Chem. Rev., 36 (1981) 325.
20 R.J. Watts, T.P. White and B.G. Griffith, J. Am. Chem. Soc., 97 (1975) 6914.
21 P.J. Giordano, S.M. Fredericks, M.S. Wrighton and D.L. Morse, J. Am. Chem. Soc., 100 (1978) 2257.
22 R.L. Blakky and M.K. DeArmond, J. Am. Chem. Soc., 109 (1987) 4895.
23 T.J. Kemp, Prog. React. Kinet., 10 (1980) 301.
24 L. Viaene and J. D'Olieslager, Inorg. Chem., 26 (1987) 960.
25 K. Kalyanasundaram, Chem Phys. Lett., 104 (1984) 357.
26 J. Higuchi, K. Suzuki, H. Arai, A. Saitoh and M. Yagi, J. Phys. Chem., 90 (1986) 1270.
27 S. Tero-Kubota, H. Oshio, T. Ito, V.L. Goedken and J. Higuchi, Chem. Phys. Lett., 131 (1986) 430.
28 J. Ferguson and F. Herren, Chem. Phys., 76 (1983) 45.
29 F. Barigelletti, A. Juris, V. Balzani, P. Belser and A. von Zelewski, Inorg. Chem., 22 (1983) 3335.
30 V.M. Miskowski, A.J. Twarowski, R.H. Fleming, G.S. Hammond and D.S. Kliger, Inorg. Chem., 17 (1978) 1056.
31 W.A. Fordyce, J.G. Brummer and G.A. Crosby, J. Am. Chem. Soc., 103 (1981) 7061.
32 C.M. Che, L.G. Butler and H.B. Gray, J. Am. Chem. Soc., 103 (1981) 7796.
33 V.M. Miskowski, G.L. Nobinger, D.S. Kliger, G.S. Hammond, N.S. Lewis, K.R. Mann and H.B. Gray, J. Am. Chem. Soc., 100 (1978) 485.
34 S.J. Milder and D.S. Kliger, J. Phys. Chem., 89 (1985) 4170.
35 A.W. Adamson, J. Chem. Educ., 60 (1983) 797.
36 G.H. Atkinson, Adv. Infrared Raman Spectrosc., 9 (1982) 1.
37 M.A. El-Sayed, Pure Appl. Chem., 57 (1985) 187.
38 S. Maeda, T. Kamisuki, H. Kataoka and Y. Adachi, Appl. Spectrosc. Rev., 21 (1985) 211.
39 S.P. McGlynn, T. Azumi and M. Kinoshita, Molecular Spectroscopy of the Triplet State, Prentice-Hall, Englewood Cliffs, NJ, 1969.
40 J.E. Wertz and J.R. Bolton, Electron Spin Resonance. Elementary Theory and Practical Applications, McGraw-Hill, New York, 1972.
41 M. Sharnoff, J. Chem. Phys., 46 (1967) 3263.
42 A.L. Kwiram, Chem. Phys. Lett., 1 (1967) 272.
43 J. Schmidt, I.A. Hesselmann, M.S. De Groot and J.H. van der Waals, Chem. Phys. Lett., 1 (1967) 434.
44 J. Schmidt and J.H. van der Waals, Chem. Phys. Lett., 2 (1968) 640.
45 M.A. El-Sayed, Izv. Akad. Nauk SSSR Ser. Phys., 37 (1973) 248.
46 M.A. El-Sayed, Adv. Photochem., 9 (1974) 311.
47 E.M. Muldakhmetov, B.F. Minaev and G.A. Kezle, Optical and Magnetic Properties of the Triplet State, Nauka, Alma-Ata, 1983 (in Russian).
48 I.Y. Chan, in R.H. Clarke (Ed.), Triplet State ODMR Spectroscopy. Techniques and Applications to Biophysical Systems, Wiley, New York, 1982, p. 1.
49 R.H. Clarke, in R.H. Clarke (Ed.), Triplet State ODMR Spectroscopy. Techniques and Applications to Biophysical Systems, Wiley, New York, 1982, p. 25.
50 R.J. Watts, J. Chem. Educ., 60 (1983) 834.
51 C.R. Jones, A.H. Maki and D.R. Kearns, J. Chem. Phys., 59 (1973) 873.

52 C.R. Jones, F. Pappano, A.H. Maki and D.R. Kearns, Chem. Phys. Lett., 13 (1972) 521.
53 H. Hayashi and S. Nagakura, Chem. Phys. Lett., 18 (1973) 63.
54 T.H. Cheng and N. Hirota, Mol. Phys., 27 (1974) 281.
55 H.J. Griesser and R. Bramley, Chem. Phys. Lett., 88 (1982) 27.
56 D.M. Burland, Chem. Phys. Lett., 70 (1980) 508.
57 G. Herzberg, Molecular Spectra and Molecular Structure, Vol. III, National Research Council of Canada, Toronto, New York, London, 1966.
58 O.F. Kalman and M.A. El-Sayed, J. Chem. Phys., 54 (1971) 4414.
59 M.A. El-Sayed, J. Chem. Phys., 54 (1971) 680.
60 D.S. Tinti and M.A. El-Sayed, J. Chem. Phys., 54 (1971) 2529.
61 C.B. Harris and R.J. Hoover, J. Chem. Phys., 56 (1972) 2199.
62 C.J. Winscom and A.H. Maki, Chem. Phys. Lett., 12 (1971) 264.
63 R.A. Avarmaa and A.P. Suisalu, Izv. Akad. Nauk SSSR Ser. Phys., 44 (1980) 843.
64 J. Schmidt, W.S. Veeman and J.H. van der Waals, Chem. Phys. Lett., 4 (1969) 341.
65 R.A. Avarmaa and A.P. Suisalu, Opt. Spektrosk., 47 (1979) 1113.
66 T.J. Schaafsma, in R.H. Clarke (Ed.), Triplet State ODMR Spectroscopy. Techniques and Applications to Biophysical Systems, Wiley, New York, 1982, p. 291.
67 S.R. Langhoff, E.R. Davidson, M. Gouterman, W.R. Leenstra and A.L. Kwiram, J. Chem. Phys., 62 (1975) 169.
68 M. Leung and M.A. El-Sayed, J. Am. Chem. Soc., 97 (1975) 669.
69 M. Gehrtz, Ch. Bräuchle and J. Voitländer, J. Photochem., 17 (1981) 7.
70 U. Steiner, J. Photochem., 17 (1981) 6.
71 D.C. Doetschman, B.J. Botter, J. Schmidt and J.H. van der Waals, Chem. Phys. Lett., 38 (1976) 18.
72 R.A. Avarmaa and A.P. Suisalu, Izv. Akad. Nauk SSSR Ser. Phys., 47 (1983) 2364.
73 I.Y. Chan, W.G. van Dorp, T.J. Schaafsma and J.H. van der Waals, Mol. Phys., 22 (1971) 741.
74 I.Y. Chan, W.G. van Dorp, T.J. Schaafsma and J.H. van der Waals, Mol. Phys., 22 (1971) 753.
75 M. Gouterman, B.S. Yamanashi and A.L. Kwiram, J. Chem. Phys., 56 (1972) 4073.
76 M. Gouterman, Porphyrins, 3 (1978) 1.
77 G.W. Canters and J.H. van der Waals, Porphyrins, 3 (1978) 531.
78 R.E. Connors and W.R. Leenstra, In R.H. Clarke (Ed.), Triplet State ODMR Spectroscopy. Techniques and Applications to Biophysical Systems, Wiley, New York, 1982, p. 257.
79 A.J. Hoff, in R.H. Clarke (Ed.), Triplet State ODMR Spectroscopy. Techniques and Applications to Biophysical Systems, Wiley, New York, 1982, p. 367.
80 D.S. McClure, J. Chem. Phys., 20 (1952) 682.
81 L.K. Hanson, M. Gouterman and J.C. Hanson, J. Am. Chem. Soc., 95 (1973) 4822.
82 R.L. Ake and M. Gouterman, Theor. Chim. Acta, 15 (1969) 20.
83 F.S. Ham, Phys. Rev. A, 138 (1965) 1727.
84 J.A. Kooter, G.W. Canters and J.H. van der Waals, Mol. Phys., 33 (1977) 1545.
85 W.G. van Dorp, T.J. Schaafsma, M. Soma and J.H. van der Waals, Chem. Phys. Lett., 21 (1973) 221.
86 R.H. Clarke and R.E. Connors, J. Chem. Phys., 62 (1975) 1600.
87 W.R. Leenstra, M. Gouterman and A.L. Kwiram, J. Chem. Phys., 68 (1978) 327.
88 G. Jansen and J.H. van der Waals, Chem. Phys. Lett., 43 (1976) 413.
89 R.E. Connors, J.C. Comer and R.R. Durand, Jr., Chem. Phys. Lett., 61 (1976) 270.
90 R.J. Platenkamp and G.W. Canters, J. Phys. Chem., 85 (1981) 56.

91 J.A. Kooter and G.W. Canters, Mol. Phys., 41 (1980) 361.
92 W.R. Leenstra, M. Gouterman and A.L. Kwiram, J. Chem. Phys., 71 (1979) 3535.
93 A.P. Suisalu and R.A. Avarmaa, Opt. Spektrosk., 60 (1986) 748.
94 R.H. Clarke and R.H. Hofeldt, J. Chem. Phys., 61 (1974) 4582.
95 W. Hägele, D. Schmid and H.C. Wolf, Z. Naturforsch. Teil A, 33 (1978) 83.
96 R.P.H. Kooyman, T.J. Schaafsma and J.F. Kleibeuker, Photochem. Photobiol., 26 (1977) 235.
97 R. Avarmaa and T.J. Schaafsma, Chem. Phys. Lett., 71 (1980) 339.
98 J.R. Norris, R.A. Uphaus and J.J. Katz, Chem. Phys. Lett., 31 (1975) 157.
99 M.C. Thurnauer and J.R. Norris, Chem. Phys. Lett., 47 (1977) 100.
100 R.H. Clarke, R.E. Connors, T.J. Schaafsma, J.F. Kleibeuker and R.J. Platenkamp, J. Am. Chem. Soc., 98 (1976) 3674.
101 R.H. Clarke and H.A. Frank, Chem. Phys. Lett., 51 (1977) 13.
102 R.H. Clarke, D.R. Hobart and W.R. Leenstra, J. Am. Chem. Soc., 101 (1979) 2416.
103 R.P.H. Kooyman, T.J. Schaafsma, G. Jansen, R.H. Clarke, D.R. Hobart and W.R. Leenstra, Chem. Phys. Lett., 68 (1979) 65.
104 W.A.J.A. van der Poel, M. Noort, J. Herbich, C.J.M. Coremans and J.H. van der Waals, Chem. Phys. Lett., 103 (1984) 245.
105 W.A.J.A. van der Poel, J. Herbich and J.H. van der Waals, Chem. Phys. Lett., 103 (1984) 253.
106 W. Barendswaard, J. van Tol and J.H. van der Waals, Chem. Phys. Lett., 121 (1985) 361.
107 R.M. Miller and D.S. Tinti, Chem. Phys. Lett., 130 (1986) 352.
108 W. Barendswaard, R.T. Weber and J.H. van der Waals, J. Chem. Phys., 87 (1987) 3731.
109 W. Barendswaard and J.H. van der Waals, Mol. Phys., 59 (1986) 337.
110 M. Yagi, A. Saitoh, K. Takano, K. Suzuki and J. Higuchi, Chem. Phys. Lett., 118 (1985) 275.
111 M. Yagi, H. Shirai, J. Ohta and J. Higuchi, Chem. Phys. Lett., 160 (1989) 13.
112 A.P. Suisalu, A.L. Kamyshny, V.N. Zakharov, L.A. Aslanov and R.A. Avarmaa, Chem. Phys. Lett., 134 (1987) 617.
113 A.P. Suisalu, L.A. Aslanov, A.L. Kamyshny, V.N. Zakharov and R.A. Avarmaa, Izv. Akad. Nauk SSSR Ser. Phys., 52 (1988) 445.
114 A.L. Kamyshny, V.N. Zakharov, L.A. Aslanov, A.P. Suisalu and R.A. Avarmaa, Koord. Khim., 15 (1989) 548.
115 Y. Komada, S. Yamauchi and N. Hirota, J. Phys. Chem., 90 (1986) 6425.
116 E. van Oort, R. Sitters, J.H. Scheijde and M. Glasbeek, Chem. Phys. Lett., 144 (1988) 2394.
117 J. Westra and M. Glasbeek, Chem. Phys. Lett., 166 (1990) 535.
118 A.L. Kamyshny, A.P. Suisalu and L.A. Aslanov, Proceedings of the All-Union Conference on Spectroscopy of Coordination Compounds, Krasnodar, USSR, 1988, p. 9 (in Russian).
119 B.M. Dzhagarov and G.P. Gurinivich, Excited Molecules. Kinetics of Transformations, Nauka, Leningrad, 1982, p. 59 (in Russian).
120 M. Gouterman, F.P. Schwarz and P.D. Smith, J. Chem. Phys., 59 (1973) 676.
121 N. van Dijk, M. Noort, S. Voelker, G.W. Canters and J.H. van der Waals, Chem. Phys. Lett., 71 (1980) 415.
122 W.G. van Dorp, G.W. Canters and J.H. van der Waals, Chem. Phys. Lett., 35 (1975) 450.
123 Y. Shimizu, Y. Tanaka and T. Azumi, J. Phys. Chem., 88 (1984) 2423.
124 Y. Tanaka and T. Azumi, Chem. Phys. Lett., 132 (1986) 357.
125 L. Bär, G. Gliemann, L. Chassot and A. von Zelewsky, Chem. Phys. Lett., 123 (1986) 264.
126 W.-H. Chen, K.E. Rieckhoff and E.-M. Voigt, Mol. Phys., 59 (1986) 355.

127 W.-H. Chen, K.E. Rieckhoff and E.-M. Voigt, Mol. Phys., 62 (1987) 541.
128 W. Halper and M.K. DeArmond, Chem. Phys. Lett., 24 (1974) 114.
129 M.I.S. Kenney, J.W. Kenney, III and G.A. Crosby, Organometallics, 5 (1986) 230.
130 W.H. Elfring, Jr. and G.A. Crosby, J. Am. Chem. Soc., 103 (1981) 2683.
131 Y. Gondo and Y. Kanda, Bull. Chem. Soc. Jpn., 38 (1965) 1187.
132 A. Harriman, J. Photochem., 8 (1978) 205.
133 K. Vinodgopal and W.R. Leenstra, J. Phys. Chem., 89 (1985) 3824.
134 M.D. Marcantonatos, M. Deschaux and J.-J. Vuilleumier, J. Chem. Soc. Faraday Trans. 2, 82 (1986) 609.
135 D.H.W. Carstens and G.A. Crosby, J. Mol. Spectrosc., 34 (1970) 113.
136 M. Nishizawa, T.M. Suzuki, S. Sprouse, R.J. Watts and P.C. Ford, Inorg. Chem., 23 (1984) 1837.
137 A.L. Kamyshny, V.N. Zakharov, L.A. Aslanov, A.P. Suisalu and R.A. Avarmaa, Opt. Spectrosk., 66 (1989) 81.
138 A.P. Suisalu, V.N. Zakharov, A.L. Kamyshny and L.A. Aslanov, Zh. Eksp. Teor. Fiz., 98 (1990) 1330.
139 L.L. Merritt and E.D. Schroeder, Acta Crystallogr., 9 (1956) 801.
140 Y. Gondo and A.H. Maki, J. Phys. Chem., 72 (1968) 3215.
141 M. Yagi, K. Makiguchi, A. Ohnuki, K. Suzuki, J. Higuchi and S. Nagase, Bull. Chem. Soc. Jpn., 58 (1985) 252.
142 R. Benedix, P. Birner, F. Birnstock, H. Hennig and H.-J. Hofmann, J. Mol. Struct., 51 (1979) 99.
143 V. Barone, F. Lelj, C. Cauletti, M.N. Piancastelli and M. Russo, Mol. Phys., 49 (1983) 599.
144 J. Higuchi, M. Yagi, T. Iwaki, M. Bunden, K. Tanigaki and T. Ito, Bull. Chem. Soc. Jpn., 53 (1980) 890.
145 M. Yagi, Y. Deguchi, Y. Shioya and J. Higuchi, Chem. Phys. Lett., 144 (1988) 412.
146 A.V. Yatsenko, V.N. Zakharov, A.L. Kamyshny and L.A. Aslanov, Koord. Khim., 15 (1989) 1114.
147 N.A. Skorik and V.N. Kumok, Chemistry of Coordination Compounds, Vysshaya Shkola, Moscow, 1975, p. 152 (in Russian).
148 P. Kuroda, Y. Sasaki and Y. Saito, Acta Crystallogr. Sect. B, 30 (1974) 2053.
149 N. Hirota, M. Baba, Y. Hirata and S. Nagaoka, J. Phys. Chem., 83 (1979) 3350.
150 S. Yamauchi, Y. Komada and N. Hirota, Chem. Phys. Lett., 129 (1986) 197.
151 H. Yersin, E. Gallhuber, G. Hensler and D. Schweitzer, Chem. Phys. Lett., 161 (1989) 315.
152 V.N. Zakharov, A.L. Kamyshny, L.A. Aslanov and A.P. Suisalu, Proceedings of the All-Union Conference on the Chemistry of Coordination Compounds, Minsk, 1990, p. 565 (in Russian).
153 W.G. van Dorp, M. Soma, J.A. Kooter and J.H. van der Waals, Mol. Phys., 28 (1974) 1551.
154 W.G. van Dorp, W.G. Schoemaker, M. Soma and J.H. van der Waals, Mol. Phys., 30 (1975) 1701.
155 S.J. van der Bent and T.J. Schaafsma, Chem. Phys. Lett., 35 (1975) 45.
156 N. Okabe, T. Ikeyama and T. Azumi, Chem. Phys. Lett., 165 (1990) 24.
157 G.P. Gurinovich, A.N. Sevchenko and K.N. Solov'ev, Spectroscopy of Chlorophyll and Related Compounds, Nauka i Tekhnica, Minsk, 1968, p. 354 (in Russian).
158 J.A. Barltrop and J.D. Coyle, Excited States in Organic Chemistry, Wiley, London, 1978.
159 F. Metz, S. Friedrich and G. Hohlneicher, Chem. Phys. Lett., 16 (1972) 353.
160 S.S. Dvornikov, V.N. Knyukshto, A.N. Sevchenko, K.N. Solov'ev and M.P. Tsvirko, Dokl. Akad. Nauk SSSR, 240 (1978) 1457.

161 S.S. Dvornikov, V.N. Knyukshto, K.N. Solov'ev and M. P. Tsvirko, Opt. Spektrosk., 46 (1979) 689.
162 M.K. DeArmond, W.L. Huang and C.M. Carlin, Inorg. Chem., 18 (1979) 3388.
163 B. Norden, R. Håkansson and M. Sundbom, Acta Chem. Scand., 26 (1972) 429.
164 S.K. Lower and M.A. El-Sayed, Chem. Rev., 66 (1966) 199.
165 I. Hanazaki and S. Nagakura, Inorg. Chem., 8 (1969) 648.
166 A. Ceulemans and L.G. Vanquickenborne, J. Am. Chem. Soc., 103 (1981) 2238.
167 I.Y. Chan, C.J. Sandroff and B.L. Goldenberg, Chem. Phys. Lett., 61 (1979) 465.
168 R. Gillies, W.U. Spendel and A.M.P. Goncalves, Chem. Phys. Lett., 66 (1979) 121.
169 A.M.P. Goncalves and R. Gillies, Chem. Phys. Lett., 69 (1980) 164.